UNIVERSITY OF CALIFORNIA SAN DIEGO

Design and Ex-Vivo Validation of a Novel, Low-Cost, Emergency Mechanical Ventilator

A thesis submitted in partial satisfaction of the requirements for the degree Master of Science

in

Bioengineering

by

Elizabeth Aeja Heyde

Committee in charge:

Professor Lonnie Petersen, Chair
Professor Adam Engler, Co-chair
Professor James Friend
Professor Kevin King

2021

The thesis of Elizabeth Aeja Heyde is approved, and it is acceptable in quality and form for publication on microfilm and electronically.

University of California San Diego

2021

DEDICATION

This thesis is dedicated to my family and friends for their endless encouragement, support, and patience with me throughout this process. I would especially like to thank my parents, Daniel Heyde, Katie North, Samuel Tucker, Patrick Arakaki, Jennifer Kandell, and Amanda Krysl. Patience is not one of my own virtues, but I am exceedingly grateful that it is something in which they all excel and have exercised generously with me over the last several months.

EPIGRAPH

Well, I’m still breathing.

Leon Spinks

TABLE OF CONTENTS

LIST OF ABBREVIATIONS

AAMI	Association for the Advancement of Medical Instruments
ACE2	Angiotensin converting enzyme 2
ARDS	Acute respiratory distress syndrome
AT-II	Alveolar type-II (type-II pneumocyte)
AVERT	Acute Ventilation Rapid Response Taskforce
BCV	Biphasic Cuirass Ventilation
BiPAP	Biphasic positive airway pressure
BMV	Bag-mask ventilation
COVID-19	2019 novel coronavirus disease
CPAP	Continuous positive airway pressure
CWP	Chest wall pressure
ERV	Expiratory reserve volume
EUA	Emergency use authorization
FDA	Food and Drug Administration
FRC	Functional residual capacity
HEPA	High efficiency particulate air
LCD	Liquid crystal display
LED	Light emitting diode
I:E	Inspiration to expiration time ratio
IPPV	Invasive positive pressure ventilation
IRV	Inspiratory reserve volume
ISO	International Standards Organization
NIPPV	Noninvasive positive pressure ventilation
NIV	Noninvasive ventilation

NPV	Negative pressure ventilation
PaO2/FiO2	Mean arterial oxygen partial pressure to fractional inspired oxygen ratio
PEEP	Positive end-expiratory pressure
PIP	Peak inspiratory pressure
PPV	Positive pressure ventilation
PWM	Pulse-width modulation
RR	Respiratory rate
RV	Residual volume
SARS-CoV-2	Severe acute respiratory syndrome coronavirus 2
TLC	Total lung capacity
TPP	Transpulmonary pressure
TV	Tidal volume
V/Q	Ventilation to perfusion ratio
VAP	Ventilator-associated pneumonia
VILI	Ventilator-induced lung injury

LIST OF SUPPLEMENTAL FILES

File 1: MADVent Supplementary Information; Heyde_MADVent_SupplementaryInformation.pdf

File 2: MADVent Ex-Vivo Validation Sample Video; Heyde_MADVent_Ex-VivoVideo.mp4

LIST OF FIGURES

LIST OF TABLES

ACKNOWLEDGEMENTS

I first would like to thank Dr. Lonnie Petersen for serving as a fantastic mentor, thesis advisor, and Principal Investigator for this project. She has provided me with more support and guidance than I could have hoped for when starting my degree. The thoughtfulness and consideration that she has shown to me and the other members of this lab are remarkable. I hope that I will be able to emulate those qualities in my social circles and forthcoming career.

I would like to thank Dr. James Friend for welcoming me into his lab space and for his support and guidance with this thesis. I would also like to acknowledge the AVERT taskforce for bringing this project to life despite the obstacles brought on by the pandemic. I would specifically like to thank Aditya Vasan, who provided advice and assistance during the execution of this project.

I would like to thank Dr. Adam Engler for serving as the Co-Chair of this thesis and for providing guidance throughout the process. I would also like to thank Dr. Kevin King for his input to this thesis.

Lastly, I would like to thank the Office of Naval Research (Grant N00014–20–P–2007), Kratos Defense and Security Solutions (Gift R–86X16–VX16) and the University of California San Diego for provision of funds and facilities in support of this work. The opinions, interpretations, conclusions, and recommendations are those of the author and are not necessarily endorsed by these parties.

ABSTRACT OF THE THESIS

Design and Ex-Vivo Validation of a Novel, Low-Cost, Emergency Mechanical Ventilator

by

Elizabeth Aeja Heyde

Master of Science in Bioengineering

University of California San Diego, 2021

Professor Lonnie Petersen, Chair
Professor Adam Engler, Co-Chair

Mechanical ventilator shortages have become increasingly frequent due to the COVID-19 pandemic. There is an unmet need for low cost, easily assembled emergency-use ventilators that are minimally susceptible to supply chain disruptions. The MADVent is a single-mode continuous, mandatory, pressure-controlled, time-terminated ventilator developed to be easily sourced and assembled for use in emergency scenarios, including COVID-induced acute respiratory distress syndrome (ARDS). This study hypothesizes that the proposed ventilator design can successfully inflate tissue for sustained

periods, with waveforms comparable to existing ventilators on the market. The main aim of this study is to determine if the MADVent Mark V can safely and effectively inflate mammalian lungs for sustained periods. Sub-aims include (1) optimizing the ventilator design for safety, efficacy, and reduced cost, (2) validating the ventilator on a mechanical lung simulator, and (3) and validating the ventilator on an ex-vivo model. Tests were completed using a mechanical lung simulator or porcine lungs as models. Pressure, flow, and volume data were collected and processed using BIOPAC's respiratory data acquisition hardware and software. Parameters including respiratory rate, inspiration time, target pressure, and compliance were varied across trials with both models to simulate various clinical conditions including extreme scenarios and long durations. Dynamic compliance of the porcine lung was calculated to be 0.037 L/cmH2O, which is comparable to the compliance applied during most mechanical model trials. The MADVent Mark V effectively mechanically ventilates both mechanical lung simulators and ex-vivo porcine models. Next steps include preparing an FDA submission.

1 INTRODUCTION

1.1 MOTIVATION

Mechanical ventilation is an essential treatment modality for many patients suffering from respiratory illness [1] [2]. These devices are often intricate, expensive, and difficult to obtain at short notice [3] [4], leading to the death or the employment of the risky, but necessary practice of splitting ventilators for multiple patients [5] [6]. There is an unmet need for low cost, easily assembled and scalable ventilators that are minimally susceptible to supply chain disruptions. This thesis is motivated by several factors including shortages of and subsequent high demand for mechanical ventilators during the COVID-19 pandemic [7], mechanical ventilator shortages that have occurred during other crises [6] [8] [9] [10], need for solutions in low-income countries [11], and novel applications of mechanical ventilation.

1.1.1 COVID-19 Pandemic

The 2019 novel coronavirus disease (COVID-19) has resulted in a global shortage of mechanical ventilators [7]. The COVID-19 outbreak was first recognized in Wuhan, China in late 2019 as the respiratory illness responsible for a series of pneumonia cases [12] [13]. Severe acute respiratory syndrome coronavirus 2 (SARS-CoV-2) is the beta coronavirus that causes COVID-19 [13]. This RNA virus is highly infectious and generally transmitted through droplets expelled by infected persons [13]. The response elicited from SARS-CoV-2 infected persons to the COVID-19 disease varies from asymptomatic to critical conditions and may even lead to death [13] [14]. A severe progression of COVID-19 and the dominant cause of mortality and morbidity for the disease includes the development of Acute Respiratory Distress Syndrome (ARDS) which precludes acute hypoxemic respiratory failure [13]. Those suffering from COVID-19 related ARDS frequently require mechanical ventilation interventions [7] [13].

COVID-19 rapidly spread across the globe causing a direct health threat to at-risk populations and the effective closure of many economies [13]. Throughout the epidemic's lifecycle, waves of COVID-19 cases have led to local excesses of persons requiring medical attention [13]. Many hospitals have experienced capacity issues due to the abnormally high demand for care and have struggled to meet the needs of front-line workers and patients alike [13] [15]. Severely symptomatic patients have been acutely impacted by scarcity of resources including Intensive Care Unit (ICU) beds and mechanical ventilators [7] [15]. Economic closures imposed to stifle the spread of SARS-CoV-2 have also stifled the global capacity to respond to resource shortages due to disruption of component supply lines, particularly for specialized equipment utilized in medical devices [16]. Adjusting manufacturing lines for ventilator production and placement of large-quantity mechanical ventilator by high-income countries has reduced shortage issues in those countries [15] [16] [17], but many low- and middle-income countries have continued to struggle to obtain these life-saving instruments [18] [19].

As of May 2021, there have been over 170,000,000 confirmed cases and over 3,500,000 confirmed deaths recorded in 223 countries, areas, or territories [20]. Although there are now several COVID-19 vaccines that have received emergency use approval (EUA) in the United States and European Union, three major variants of the virus have emerged with varying resistance to available vaccines [21]. With the ongoing deployment of vaccines in high-income countries, inconsistent availability of vaccines in low- and middle-income countries, and the uncertainty surrounding the efficacy of already delivered vaccines, it is pertinent to continue improving the accessibility and reliability of respiratory support devices for treatment of COVID-19 induced ARDS and related complications.

1.1.2 Additional Ventilator Shortages and Needs

The COVID-19 pandemic is only the most recent cause of mechanical ventilator shortages. There are numerous past crises that have caused similar supply deficiencies, although most of these incidents have been more localized and were impactful for shorter spans of time. Public health emergencies may

include severe influenza outbreaks [8] [9], mass shootings or massacres [6], and severe weather or natural disasters [10]. Low-income countries are at increased risk of ventilator shortages in a variety of scenarios due to pre-existing medical supply shortages or limitations [11]. Without prompt regional or foreign aid responses or the ability to efficiently acquire or manufacture emergency mechanical ventilators, patients with respiratory trauma or disease are at increased risk of mortality [11] [22]. An inexpensive, simply sourced, and easily manufacturable mechanical ventilator could drastically increase chances of survival for critical patients in any of these scenarios.

1.1.3 Out-of-hospital Use

There are numerous first aid scenarios where patients may require external support during the breathing process [23] [24]. Manual ventilation is often required to stabilize patients at the site of an emergency and en route to a medical facility [23] [24]. In these scenarios, a member of the response team is allocated to manually ventilate the patient and inaccessible for other urgent, necessary tasks [23] [24]. The application of a portable emergency ventilator to out-of-hospital scenarios would allow response teams to focus their attention on other essential tasks and towards the diagnosis of underlying causes of the respiratory malfunction, and would provide more consistent, controlled ventilatory action [25]. Similar devices have been successfully implemented to automate chest compressions in other emergency scenarios [26].

1.2 Hypothesis and Aims

The hypothesis for this study is that the proposed MADVent Mark V, hereafter referred to as MADVent, design developed by the University of California San Diego Acute Ventilation Rapid Response Taskforce (AVERT) can successfully inflate tissue for sustained periods, with waveforms comparable to existing ventilators on the market. The overarching aim of this thesis is to complete a series

of validation studies culminating in the execution of an ex-vivo study using a porcine lung. This goal has been broken down into the following sub-aims:

1. Ensure that the MADVent is safe, effective, low-cost, and easily manufacturable.
2. Assess the safety and efficacy of the MADVent using a mechanical lung simulator.
3. Assess the safety and efficacy of the MADVent using an ex-vivo model.

The finalized MADVent design will be submitted to the FDA under a 510k submission. Validation using fixated mammalian tissue and against existing ventilators will support the function of this model and suggest readiness for in-person use.

2 BACKGROUND

The objective of this section is to provide the necessary background required for understanding pulmonary physiology and mechanics, the mechanics of mechanical ventilation, and currently existing mechanical ventilation technologies.

2.1 PULMONARY ANATOMY AND PHYSIOLOGY

The primary function of the pulmonary system is to facilitate gas exchange between the air and pulmonary vasculature [27] [28]. This section will provide an overview of respiratory anatomy and physiology and will discuss some specific concepts pertaining to pulmonary function.

2.1.1 Gross Anatomy and Physiology

The respiratory system resides primarily in the thoracic cavity and is often discussed in terms of the upper airways and lung parenchyma [27] [28]. The upper airways, or conduction zone, consist of the nasal and oral cavities, pharynx, and larynx [27] [28]. These structures filter and heat ambient oxygenated air during inspiration and allow for expulsion of carbon dioxide during expiration [27] [29]. The lower structures comprising the respiratory zone broadly include the lungs and tracheobronchial tree, which successively differentiates from the trachea into bronchi, bronchioles, and alveoli [27] [28] [29]. The right, larger lung includes superior, middle, and inferior lobes; while the left lobe includes superior and inferior lobes and a cardiac notch to accommodate the heart [27] [28] [29] [30]. The lungs are protected by the ribcage and have bases that rest on the diaphragm [27] [28]. The major anatomical structures of the respiratory system can be seen in Figure 1.

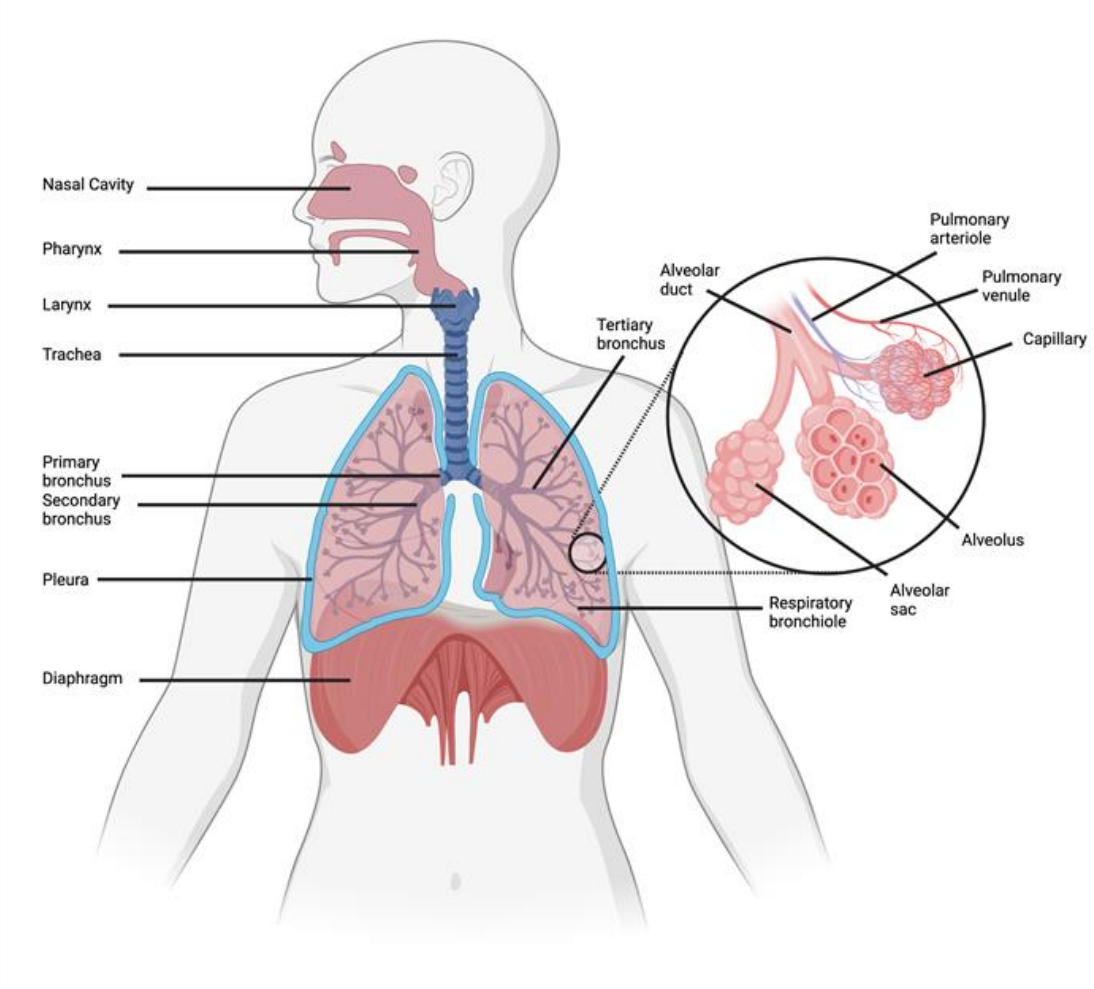

Figure 1: A graphical representation of the major structures of the respiratory system [29].

Inspiration or inhalation is actuated by the synchronized downward movement of the diaphragm and upward movement of the external intercostals [31]. Expiration or exhalation is conversely generated during the passive, elastic recoil of the inhalation muscles, but may include the additional contraction of the internal intercostals and abdominal muscles during forced expiration [31]. The volume changes accompanying the expansion and contraction of the thoracic cavity and consequently the lungs, introduces a gradient between intrapulmonary and atmospheric pressures that causes flow through the system [28] [31]. Accessory inspiratory and expiratory muscles including the sternocleidomastoids and scalene muscles may further expand and contract the thoracic cavity [28]. Accessory muscle engagement intensifies during respiratory distress or failure events [28].

A pleural sac individually encases each lung, with the visceral pleura attaching directly to the lung and the parietal pleura connecting to the thoracic wall, mediastinum, and diaphragm [28] [30] [31]. The pleural cavity contains serous pleural fluid that both minimizes friction between the walls during breathing and maintains contact between the lung and thoracic wall and bordering muscles via cohesion [30]. The intrapleural pressure describes the pressure maintained within the pleural fluid with respect to atmospheric pressure, about -4mmHg at rest [31]. This difference is often equivalent to the chest wall pressure (CWP), the difference between the intrapleural and pressure on the body surface [31]. The transpulmonary pressure (TPP), or the difference between the intrapleural and intrapulmonary pressures, neutralizes the outward elastic recoils of the chest wall using the inward elastic recoil of the lung [31]. At complete rest, TPP and CWP are equal and prevent flow [31]. Compliance can be impacted by the changes in TPP and is discussed further, later in this section [31].

Gas exchange takes place across the thin alveolar walls to the blood in the pulmonary capillaries [27] [28] [30] [32]. The rapid diffusion across this barrier is driven primarily by the concentration gradients of oxygen and carbon dioxide, but can also be impacted by the surface area of the alveoli and membrane thickness [32]. Since gas exchange is normally perfusion-limited, the airflow through the lungs to the alveoli and perfusion of blood into the capillary bed are frequently compared using a ventilation to perfusion ratio (V/Q) [32]. The V/Q measures close to 1 at the middle of the lung, with higher and lower values at the base and apex, respectively [33]. While the V/Q normally differs throughout the lung, significant changes to this ratio can lead to conditions like hypoxemia and hypercapnia [32].

2.1.2 Respiratory Volumes

Respiratory action can be described in terms of the capacities of the system and the volume of air currently within the system. The definitions of the main volumes and capacities, the normal reference values for healthy adults, and pertinent calculations (Equations 1, 2, 3, and 4) are detailed in Table 1.

Table 1: Lung volumes and capacities, definitions, and normal reference values for healthy adults [34].

Term	Definition	Normal reference values for healthy adults (mL/kg)
Inspiratory reserve volume (IRV)	Maximum volume increase over tidal volume attained by forced inspiration	45
Tidal volume (TV)	Normal volume inspired/expired during quiet breathing	7
Expiratory reserve volume (ERV)	Maximum volume decrease attained by forced expiration	15
Residual volume (RV)	Volume remaining in the lung after forced expiration	15
Total lung capacity (TLC)	Total volume the lung can hold $TLC = IRV + TV + ERV + RV$ (1) TLC is total lung capacity IRV is inspiratory reserve volume TV is tidal volume ERV is expiratory reserve volume RV is residual volume	82
Vital capacity (VC)	Maximum volume change between forced inspiration and forced expiration $VC = IRV + TV + ERV$ (2) VC is vital capacity	67
Inspiratory capacity (IC)	Maximum volume increase attained by forced inspiration $IC = IRV + TV$ (3) IC is inspiratory capacity	52
Functional residual capacity (FRC)	Total volume remaining in the lung after quiet expiration $FRC = ERV + RV$ (4) FRC is functional residual capacity	30

A visual representation of these capacities and volumes, and their average value ranges for healthy adults measured using spirometry, can be seen in Figure 2.

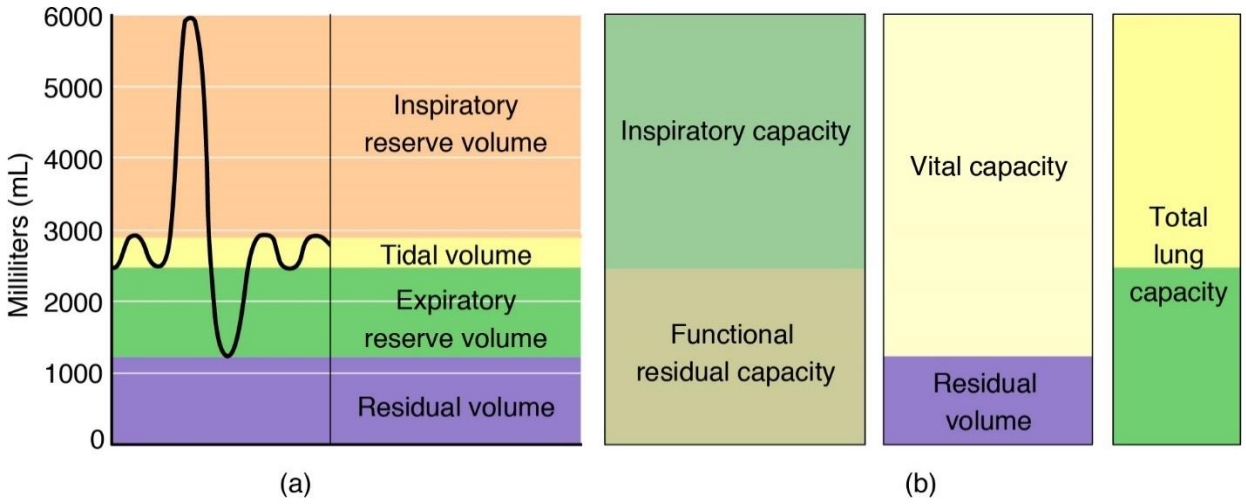

Figure 2: Visual representation of the lung (a) volumes and (b) capacities [27].

2.1.3 Flow, Resistance, and Dead Space

Flow throughout the airways is approximated as laminar during normal breathing and can be described by the Hagen-Poiseuille equation (Equation 5) [35] [36]. Large diameter airways with irregular walls such as found in the trachea, high velocity flows as experienced in many exercises, and diseases may cause significant turbulent flows to emerge where the Hagen-Poiseuille relationships become irrelevant [35].

$$Q = \frac{\pi \Delta P r^4}{8 L \eta} \tag{5}$$

Q is flow
ΔP is pressure gradient
r is radius
L is vessel length
η is viscosity

The relationship between flow, pressure, and resistance is described by Ohm's law (Equation 6), which can be combined with the Hagen-Poiseuille equation to determine resistance (Equation 7) [36].

$$Q = \frac{\Delta P}{R} \tag{6}$$

$$R = \frac{8\eta L}{\pi r^4} \tag{7}$$

R is resistance

Although flow is not perfectly laminar, especially under pathophysiological conditions, the Hagen-Poiseuille equation can still be used to show the relationships between the different vessel parameters and to emphasize how small changes in vessel radius significantly impact the resistance of the airway [35] [36]. Resistance is minimized during inspiration due to the increased radius of the airways, and is maximized during expiration when recoil occurs [36]. The parallel bronchi airways have the lowest cumulative radius and consequently the highest resistance of the various airways [36]. These passages are therefore most susceptible to significant increases in resistance with the onset of disease, which may result in increased dead space within the system [36].

The dead space is comprised of the volume of ventilated air that does not undergo gas exchange [37] [38]. Anatomical dead space consists of the volume from the nasal and oral cavities to the bronchi, while the alveolar dead space encompasses the volume from the bronchioles to the alveoli [37] [38]. The anatomical and alveolar dead spaces together make up the physiologic dead space (Equation 8), which is typically about one third of the total respiratory volume [37] [38].

$$VD_{Phys} = VD_{Ana} + VD_{Alv} \tag{8}$$

VD_{Phys} is physiological dead space volume
VD_{Ana} is anatomical dead space volume
VD_{Alv} is alveolar dead space volume

The Bohr equation calculates the theoretical ratio of airway dead space (Equation 9) [39].

$$\frac{VD_{Phys}}{V_T} = \frac{PACO_2 - P_ECO_2}{PACO_2} \tag{9}$$

$PACO_2$ is alveolar CO_2 pressure
P_ECO_2 is expired CO_2 pressure

The Enghoff modification of the Bohr equation, which uses arterial CO_2 pressure rather than alveolar CO_2 pressure, is frequently employed in practice to calculate the dead space since the arterial CO_2 pressure is more conveniently measured (Equation 10) [39].

$$\frac{VD_{Phys}}{V_T} = \frac{PaCO_2 - P_ECO_2}{PaCO_2} \tag{10}$$

$PaCO_2$ is arterial CO_2 pressure

The arterial CO_2 is known to be slightly larger than alveolar CO_2 pressure, but is a comparable and accessible way to determine physiological dead space in most scenarios, excluding cases involving severe intrapulmonary shunts or decreases in diffusion [39]. The Bohr or Enghoff equations can be combined with Fowler's Method of determining anatomical dead space, to calculate the effective alveolar dead space [39]. The alveolar dead space is negligible in healthy respiratory systems but may become significant if the system becomes diseased [37] [38] [39].

2.1.4 Compliance

Compliance is often used instead of its inverse, stiffness, to describe how tissue responds to an applied force [40] [41]. Pulmonary compliance is defined as the change in volume divided by the change in transpulmonary pressure (Equation 11), or the slope of the pressure-volume curve [40] [41].

$$C = \frac{\Delta V}{\Delta P} \tag{11}$$

C is compliance
ΔV is change in intrapulmonary volume
ΔP is change in intrapulmonary pressure

Compliance varies throughout the breathing cycle, where hysteresis causes compliance during expiration to exceed that of inspiration at a given pressure [40]. Compliance also depends on whether the system is dynamic (Equation 12) or static (Equation 13) since the former is dependent on the peak inspiratory pressure (PIP) and the latter is dependent on the plateau pressure (P_{Plat}) [40].

$$C_{Dynamic} = \frac{V_T}{PIP - PEEP} \tag{12}$$

$$C_{Static} = \frac{V_T}{P_{Plat} - PEEP} \tag{13}$$

$C_{Dynamic}$ is dynamic compliance
C_{Static} is static compliance
PIP is the peak inspiratory pressure
P_{Plat} is the plateau pressure
$PEEP$ is the positive-end expiratory pressure

This propensity of material to deform under load is most notably influenced by the elastin content of the tissue and the surface tension of the fluid lining the alveoli [40] [41]. While greater elastin content improves compliance, the elastin content reduces elastance, or elastic resistance, of the tissue [40] [41].

2.1.5 Surface Tension and Surfactant

Fluid lining the inside of the alveoli, comprised largely of water, creates a surface tension that pulls the alveolar walls inward and comprises part of the recoil force that allows for expiration [42]. Alveolar collapse, or atelectasis, can cause damage to the individual alveoli and reduces the surface area

available for gas exchange within the lungs [42]. The pressure required to induce atelectasis is described by the law of Laplace (Equation 14), where the surface tension comprises the hoop stress [42].

$$P_C = \frac{2\gamma}{r_A} \tag{14}$$

P_C is collapse pressure
γ is surface tension
r_A is alveoli radius

The alveoli are not perfectly spherical or independent structures, rendering Equation 14 an approximated description rather than an exact definition [43]. Normally, a pulmonary surfactant secreted by type-II pneumocytes, also called type-II alveolar cells (AT-II), disrupts and reduces the alveolar surface tension [42]. Reduction of surfactant secretion or inactivation of existing surfactant, and the consequent increase in the collapse pressure causes complications ranging from reduction in alveoli radii and reduced V/Q ratio to atelectasis [44]. ARDS, other lung diseases, and mechanical ventilation may all have a negative impact on surfactant production and activity [42] [44] [45]. Positive end-expiratory pressure (PEEP), discussed later in 2.2.3, is used to maintain intrapulmonary pressure and to oppose the collapse pressure during mechanical ventilation [42] [44].

2.1.6 Acute Respiratory Distress Syndrome

Acute respiratory distress syndrome (ARDS) is an inflammatory response to numerous injuries or disorders that ultimately leads to hypoxemia [44]. Diagnosis of ARDS using the Berlin definition occurs when PaO2/FiO2 (arterial oxygen pressure/ fraction of inspired oxygen) decays to 200 or lower [46]. The syndrome is characterized by increased pulmonary capillary permeability, surfactant deactivation, edema fluid build-up in the alveoli, and alveolar recruitment and decruitment during successive breaths [44]. Each of these characteristic malfunctions compound one another, causing a ruthless, rapid cycle of worsening respiration [44] [46] [47].

COVID-19 is one of the conditions that precedes ARDS, with the resulting ARDS closely resembling classical ARDS [48]. SARS-CoV-2 targets angiotensin-converting enzyme 2 (ACE2) receptors that are commonly found on AT-II epithelial cells [13]. One of the immune responses is an increase in the vascular permeability and inducing pulmonary edema, both of which are identifying symptoms of ARDS [13]. COVID-19-associated ARDS has shown evidence of less decreased compliance than classical ARDS and concurrent high D-dimer concentrations that are not found in classical ARDS [48]. Classical ARDS phenotypes have been most frequently differentiated by presence or absence of hyperinflammation, an indicator associated with mortality and response to treatments including mechanical ventilation [49]. COVID-19 associated ARDS has similarly been classified into two phenotypes with the Class 2 phenotype yielding almost double the mortality of the Class 1 phenotype [49]. However, the most significant differences between the classes involved vascular indicators and there were no major respiratory differences between the two groups [49].

Various combinations of reductions in surfactant, compliance, and diffusion rate and increases in surface tension, dead space, and V/Q have left ARDS patients with a mortality rate of 40% [46]. Mechanical ventilation remains the standard-of-care for ARDS, but proper low tidal volume ventilation methods must be employed to avoid overdistension and ventilator-induced lung injury (VILI) [44] . Failure to do so aggravates the existing symptoms by further exacerbating surfactant deactivation, reducing surfactant production, and straining tissue [44] [46] [47].

2.2 Mechanical Ventilation Methods

Mechanical ventilation is used to help patients breathe when they can no longer effectively breathe autonomously. This section will briefly discuss different types of mechanical ventilation, methods of controlling ventilation and their associated parameters, and existing ventilators.

Mechanical ventilation interventions may become necessary due to trauma or illness and can vary in invasiveness depending on the condition severity and site of care. The two main methods of

mechanical ventilation are negative pressure and positive pressure; these methods can be further divided into specific ventilation techniques [50]. Figure 3 contains a tree diagram listing the different methods.

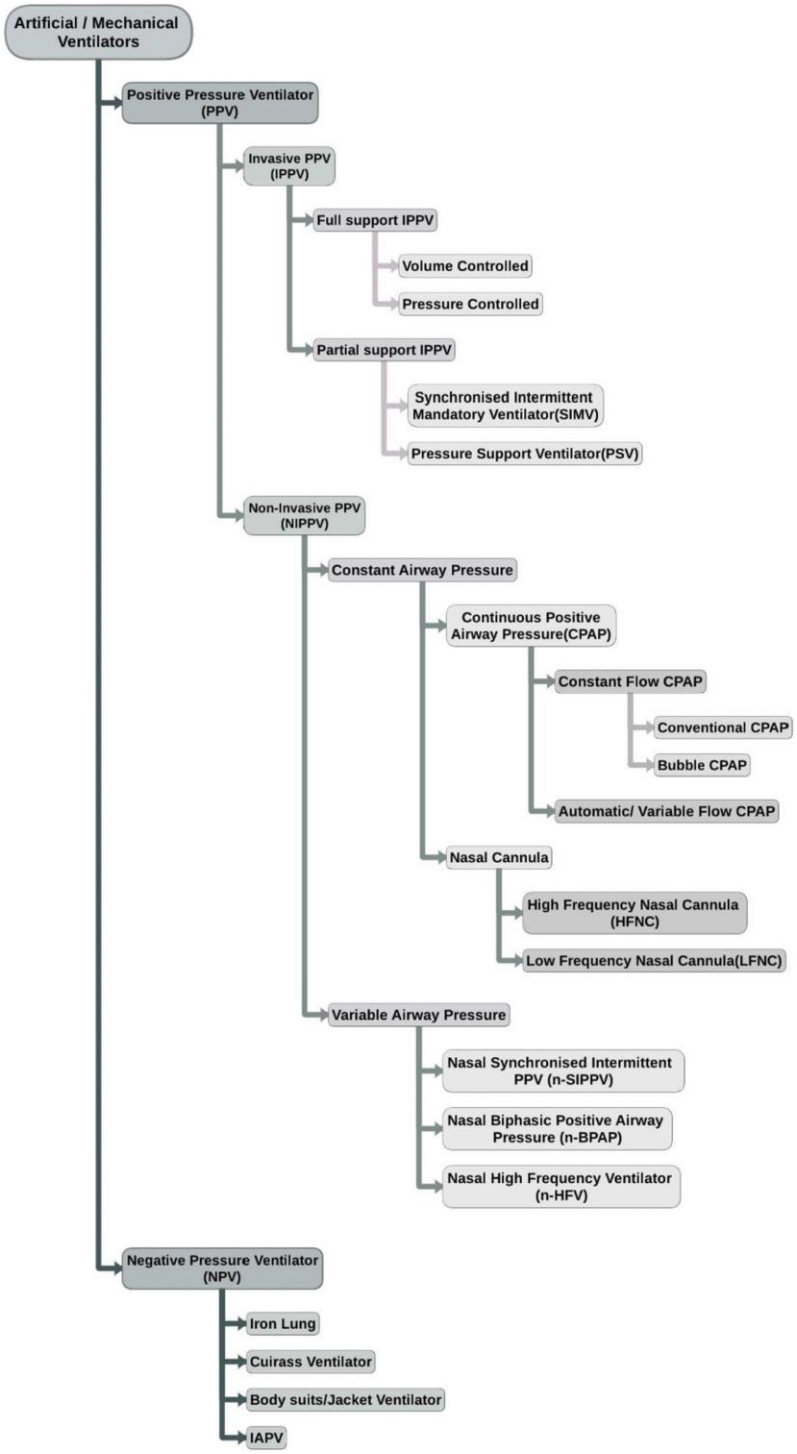

Figure 3: A tree diagram representation of mechanical ventilation categories and methods [50].

2.2.1 Negative Pressure Ventilation (NPV)

The first mechanical ventilators were developed by creating negative pressure within the system [50] [51]. Negative pressure ventilation (NPV) devices like the Iron Lung enclosed the everything but the patient's head and neck and used vacuum pumps to cyclically lower the chamber's overall pressure and then return the system to ambient pressure [51]. The pressure gradient expands the chest and pulls air into the patient's lungs when the negative pressure is applied and then passively allows for expiration as the negative pressure equilibrates [51]. Chambers like the Iron Lung, while novel for their time and not directly invasive, were straining on other organs and impeded other medical care [51]. The common modern NPV intervention is Biphasic Cuirass Ventilation (BCV) [50] [51]. BCV functions similarly to the iron lung with a much smaller chamber that only encompasses the torso [51]. These methods, along with jacket ventilators and intermittent abdominal pressure ventilators, are noninvasive but generally used for home care and those with long-term disorders [51].

2.2.2 Positive Pressure Ventilation (PPV)

Positive pressure devices comprise the vast majority of mechanical ventilator's used today [52]. Positive pressure ventilation (PPV) directly pushes air into the lungs using a positive pressure gradient rather than creating a negative pressure vacuum as in NPV and normal breathing [52]. Noninvasive ventilation (NIV) is primarily used in emergency, minor, and neonatal care [52]. Invasive ventilation is generally used in tandem with a mechanical ventilator that completely controls the respiratory cycle [52].

Noninvasive positive pressure ventilation (NIPPV) methods usually use oronasal masks to seal the path between a mechanical ventilator and the lungs [52]. The two main types of NIPPV are continuous positive airway pressure (CPAP) and biphasic positive airway pressure (BiPAP) [52]. CPAP is used in more minor cases and provides a constant positive pressure to support patient respiration. CPAP recruits alveoli that may have collapsed or are at risk of collapse, improves oxygen flow, and reduces the

work of breathing [52]. BiPAP functions similarly to CPAP but alternates the applied positive pressures during inspiration and expiration to emphasize ventilation and alveoli recruitment, respectively [52]. Both CPAP and BiPAP are assistive ventilators that support existing respiration rather than strictly controlling the entire breath [52].

In emergency scenarios outside of a care facility, bag-mask ventilation (BMV) is employed and is facilitated by a health care professional [23] [24]. This PPV method may utilize a flow-inflating or self-inflating bag [24]. Although flow-inflating bags do have CPAP functionality, they are often only used within hospitals due to their need for a pressurized gas source [24]. Self-inflating bags will refill using ambient air or with external gas sources. BMV is effective but requires one or more trained facilitators for safe operation and cannot be sustained for extended lengths of time [24].

Invasive positive pressure ventilation (IPPV) involves the insertion of a tube into the trachea through endotracheal intubation or tracheostomy [52] [53]. Endotracheal intubation refers to the process of inserting a tube through the mouth or nose to the area above the tracheal bifurcation and often requires that the patient be sedated [53]. In the occasion that the airway is obstructed or damaged, an additional, direct opening to the trachea is created via tracheostomy [53]. The exposed end of endotracheal and tracheostomy tubes may be connected to mechanical ventilators depending on the purpose of the procedure and the condition of the patient [53]. These interventions can be used for short- or long-term care [53].

Apart from assisted and support breath ventilators like CPAP and BiPAP, PPV devices offer full support and regulation of entire breathing cycle using pressure-control or volume-control [1] [54]. Pressure-controlled ventilators mimic inspiration by pushing air through the system until a threshold pressure is reached [1] [54]. Pressure builds quickly and is maintained until a timer triggers the release [1] [54]. Volume-controlled ventilators alternatively mimic inspiration by pushing a fixed volume of air through the system [1] [54]. In these systems, flow pattern is also controlled [1] [54]. There are some dual control systems, like pressure regulated volume control systems, that utilize both controls but preferentially use one method over the other [54]. Feedback mechanisms can also be incorporated to

automatically adjust the flow to the patient's needs [54]. The method of control has notable impact on the waveforms produced during ventilation; these changes are discussed in greater detail in 2.2.5 [54].

2.2.3 Positive End-Expiratory Pressure (PEEP)

Positive end-expiratory pressure (PEEP) is a crucial component of both noninvasive and invasive ventilation devices [55]. PEEP is a baseline intrapulmonary pressure at the end of exhalation that exceeds atmospheric pressure and is sometimes referred to as back pressure [55]. Properly applied PEEP helps to improve oxygenation, correct V/Q, reduce the risk of atelectasis, and reduce the effort of breathing [55]. PEEP is usually maintained with a threshold resistance valve that typically ranges from 5 to 20 cmH2O [55]. For COVID-19-associated ARDS patients, evidence demonstrates that higher PEEP (15-20 cmH2O) may be optimal for improving oxygenation [56]. Too much PEEP may cause overdistension and can also negatively affect right atrial pressure and venous return [55].

Auto-PEEP is a mechanical ventilation complication that occurs when air is unintentionally trapped within the lungs during passive expiration [55]. This trapped air creates a positive pressure that increases work required to cycle air through the lungs, V/Q, plateau pressure, and respiratory rate which leads to further auto-PEEP [54] [55].

2.2.4 Parameters

Full support ventilators are governed by a set of input parameters that specify function and serve as safeguards. These parameters are described in Table 2.

Table 2: Mechanical ventilation parameters and their definitions [1].

Term	Definition
Inspiration-expiration ratio (I:E)	the ventilation cycle time is composed of the combined inspiration and expiration time components. This inspiration and expiration time components are often expressed using the ration I:E. This ratio is approximately 1:3, but the expiration time may be increased to ensure enough time for exhalation and avoid auto-PEEP.
Respiratory rate (RR)	the frequency of ventilation defined as breaths per unit time. Average ventilator respiratory rates are about 12 bpm. Respiratory rate may be increased if oxygenation is too low.
Tidal volume (TV)	the volume delivered to the system during each breath. This value may vary or may remain constant depending on the type of control used. It is essential that the volume chosen is not too large to reduce the risk of ventilator induced lung injury. For ARDS patients, Equations 15 and 16 are used to determine the predicted body weight (PBW) of males and females, respectively, and Equation 17 is used to determine tidal volume [2]. $$Male: PBW(kg) = 50.0 + 0.905 \times (height(cm) - 152.4) \quad (15)$$ $$Female: PBW(kg) = 45.5 + 0.905 \times (height(cm) - 152.4) \quad (16)$$ $$V_T = 6\frac{mL}{kg} \times PBW \quad (17)$$ PBW is the surface tension Equation 17 is merely a guide; for patients with low lung compliance, the output tidal volume may still be too large [2].
Positive end-expiratory pressure (PEEP)	See 2.2.3. The positive pressure maintained at the end of is kept low (3-5 cmH2O) for many patients, but there is evidence that high PEEP (15-20 cmH2O) may benefit those with ARDS [2]. To avoid auto-PEEP, it is recommended to start with low PEEP and to increase, as necessary.
PaO2:FiO2	Ratio of the partial pressure of arterial oxygen to fraction of inspired oxygen. FiO2 value may be as high as 100% when first introducing ventilation and is reduced as needed.

2.2.5 Waveforms

The key waveform outputs of ventilation are differential pressure, flow, and volume [1] [54]. These parameters are frequently plotted against time, but pressure and flow are occasionally plotted against volume [1] [54]. There are characteristic qualities of each of these curves, but some variation can occur based on whether the ventilator is pressure- or volume-controlled [1] [54]. Key features of pressure waveforms also include peak inspiratory pressure (PIP) and plateau pressure (P_{Plat}) [1]. PIP refers to the maximum pressure reached during inspiration [1]. Plateau pressure refers to the pressure in the absence of airflow and at the end of inspiration; this can be seen during a breath hold [1].

Pressure curves have baseline values greater than or equal to zero [54]. Baselines that exceed zero reflect the amount of PEEP applied by the ventilator [54]. For ventilator-initiated breaths characteristic of full support IPPVs, the pressure curve increases continuously from the baseline to the PIP during inspiration and decreases rapidly during the expiration phase of the breath [54]. In pressure-controlled ventilation, pressure rises rapidly and tends to form square waveforms [54]. In volume-controlled ventilation, pressure rises more gradually and takes on a wave-like shape [54].

Volume curves have baseline values that are approximately zero [54]. End of expiration values above zero indicate expiratory leaks and values below zero indicate active exhalation [54]. In pressure-controlled ventilation, volume curves are dependent on the pressure and have variable rates of increase during inspiration [54]. In volume-controlled ventilation, the inspiratory portion of volume curve increases at a constant rate until the desired volume is achieved [54]. In both scenarios, volume drops rapidly during expiration [54].

Flow curves always cross the x-axis throughout the breath [54]. During inspiration, flow is positive and can take on a variety of shapes [54]. During expiration, flow tends to have a single negative peak that gradually ascends back up to zero [54]. In pressure-controlled ventilation, flow is a dependent variable with similar variations as volume curves [54]. In volume-controlled ventilation, clinicians can choose square, decelerating ramp, descending ramp, or sine flow patterns [54]. There are not enough studies that have been completed to concretely distinguish the advantages and disadvantages of the

different flow patterns in various treatment scenarios [54]. Flow and volume are intimately related, where volume is usually calculated as the integral of the flow [54]. Figure 4 shows examples of pressure, volume, and flow curves for both pressure- and volume-controlled ventilation.

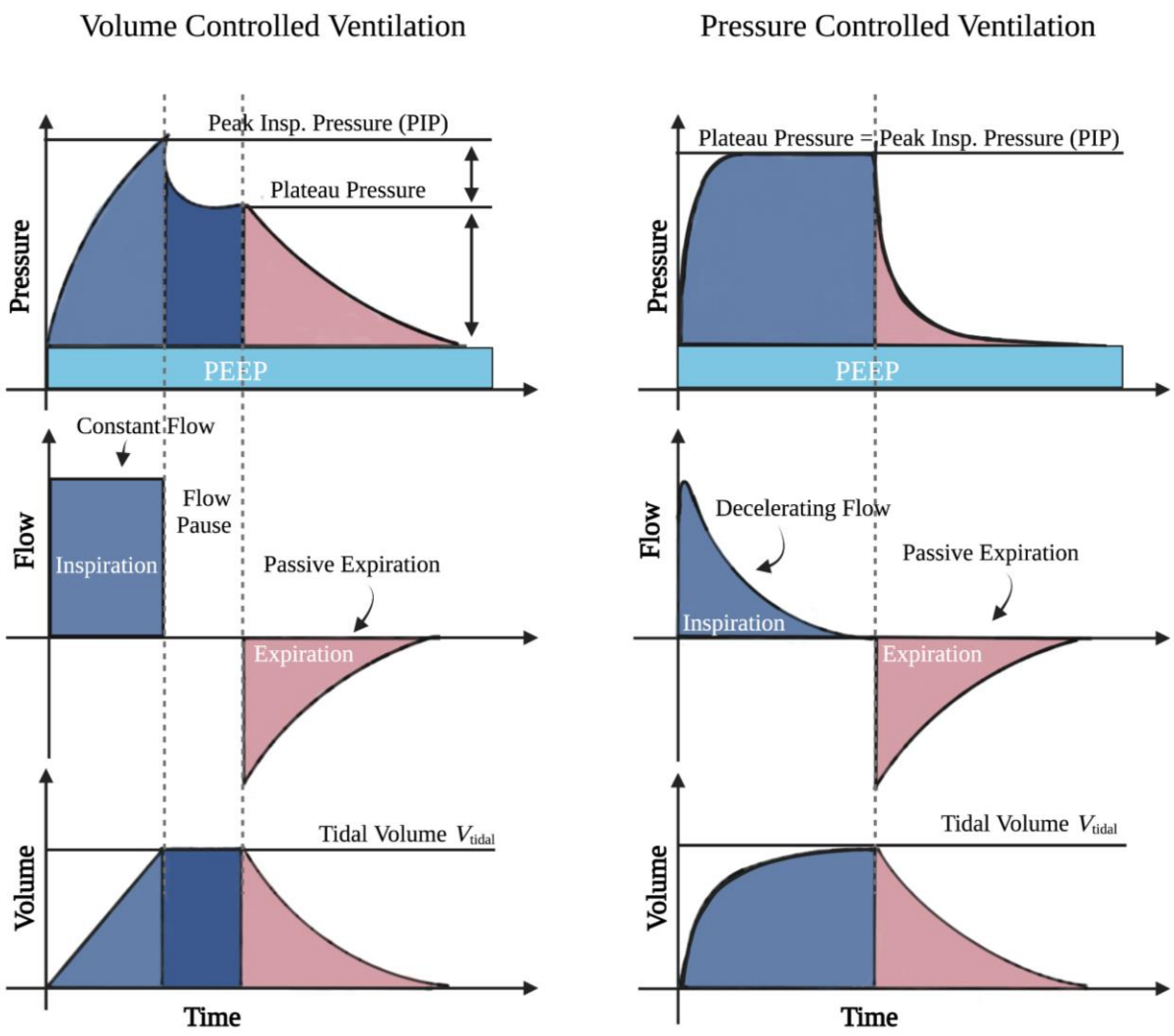

Figure 4: Comparison of pressure, flow, and volume curves for volume-controlled (left) and pressure-controlled (right) ventilation systems [57].

2.2.6 Risks

Mechanical ventilation is a necessary intervention for many patients but may involve substantial risk [58]. VILI may include, but is not limited, the following: volutrauma (alveolar overdistension), barotrauma, repetitive inflation and collapse of the alveoli, auto-PEEP, surfactant deactivation, ARDS, atelectasis, and pneumothorax [58]. Risk of VILI may be reduced by incorporating safety measures into the ventilators themselves, using preventative ventilation parameters, and strategic patient positioning [58]. Ventilator-associated pneumonia (VAP) is also a risk, particularly for patients of advanced age or prolonged mechanical ventilation treatment [58]. In some cases, patients may become reliant on artificial ventilation and will require long-term breathing assistance [58]. As with many medical interventions, mechanical ventilation increases a patient's risk of infection by introducing an artificial airway that may not adequately filter the respiratory tract [58].

2.2.7 Cost

Ventilators are expensive and difficult to acquire in a short time frame. Depending on the acuity of the ventilator, healthcare facilities can expect to pay between $5,000 and $50,000 per unit [3]. Premium ventilators commonly found in hospitals and ICUs in the United States typically sit at the higher end of this range, with most models exceeding $25,000 [3]. Portable models that service subacute and skilled nursing facilities start around $5,000 and reach up to $15,000 [4]. Service warranties may also add up to $5,000 per contract [4]. Oxygen, filters, replacement parts, and operator training also increase mechanical ventilation costs over time [4].

3 DESIGN

The objective of this section is to describe the design of and validation for the MADVent. This design focuses on an ease of-assembly, simple low-cost mechanisms, and easily sourced materials. The design is streamlined to perform essential functions using a minimal number of adjustable settings and to ensure safety with essential alarms. The ventilator aims to meet the United States Food and Drug Administration (FDA) standards for safety and efficacy and was developed in accordance with the International Standards Organization (ISO) and Association for the Advancement of Medical Instruments (AAMI) for pressure-controlled ventilation. The MADVent is a single-mode continuous, mandatory, pressure-controlled, time-terminated device. The MADVent design is best discussed in terms of its mechanical and software components. The overall design can be seen attached to a mechanical test lung; see Figure 5.

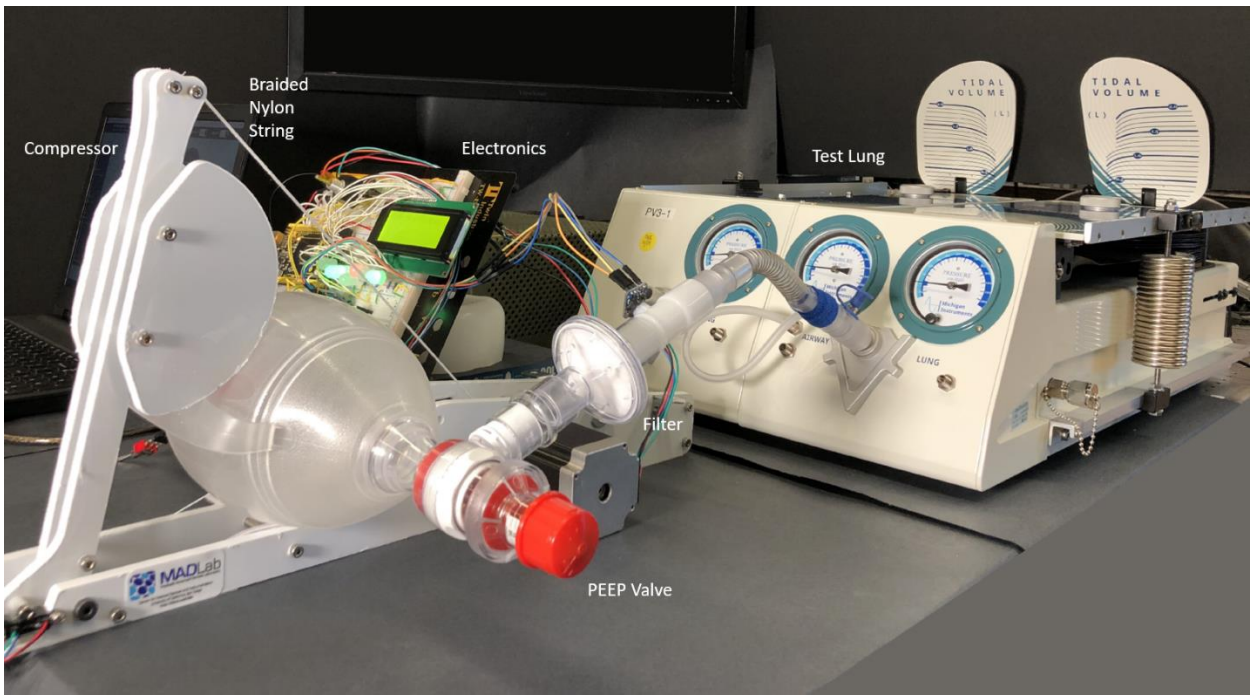

Figure 5: Illustration of MADVent Mark V

3.1 MECHANICAL DESIGN

The mechanical design of the MADVent focused on ease of assembly, simplicity, and low-cost easily sourced materials. There are two main mechanical features of the ventilator include the frame and pulley mechanism, and the self-inflating manual resuscitation bag (SPUR II, Ambu Inc, MD, USA).

3.1.1 Frame and Pulley System

The MADVent frame consists of six laser cut components: two long bases, two lever arms, and two convex compressors (Parts 1, 3, 6, 8, 9, 12 in Figure 6). All major components including the lever arms, resuscitation bag, battery, and electronics box are secured along the base structure to maximize MADVent's portability. The electronic portions of the device are primarily located at the front of the base. The lever arms and associated compressors are alternatively secured to the back of the base via a torsional spring.

The lever arms are actuated by a braided nylon lanyard that wraps around a spool attached to the motor (Figure 7). Nylon was selected for the lanyard material due to its well-known durability. As the spool winds, the lever arms descend and the compressors deflate the resuscitation bag, producing inspiration. Similarly, unspooling of the motor combined with the torsional spring allow for expiration and refilling of the resuscitation bag. The pulley mechanism employed here contrasts the gear or cam systems utilized by other low-cost ventilators. The pulley's lever arm length significantly decreases the complexity of the system by allowing greater torque to be applied to the resuscitation bag. The choice of pulley mechanism reduces wear that frequently occurs with gears and eliminates backlash. This design also limits system noises to those produced by the motor, which is notably softer than the gear rack and pinion designs and therefor more ideal for medical care.

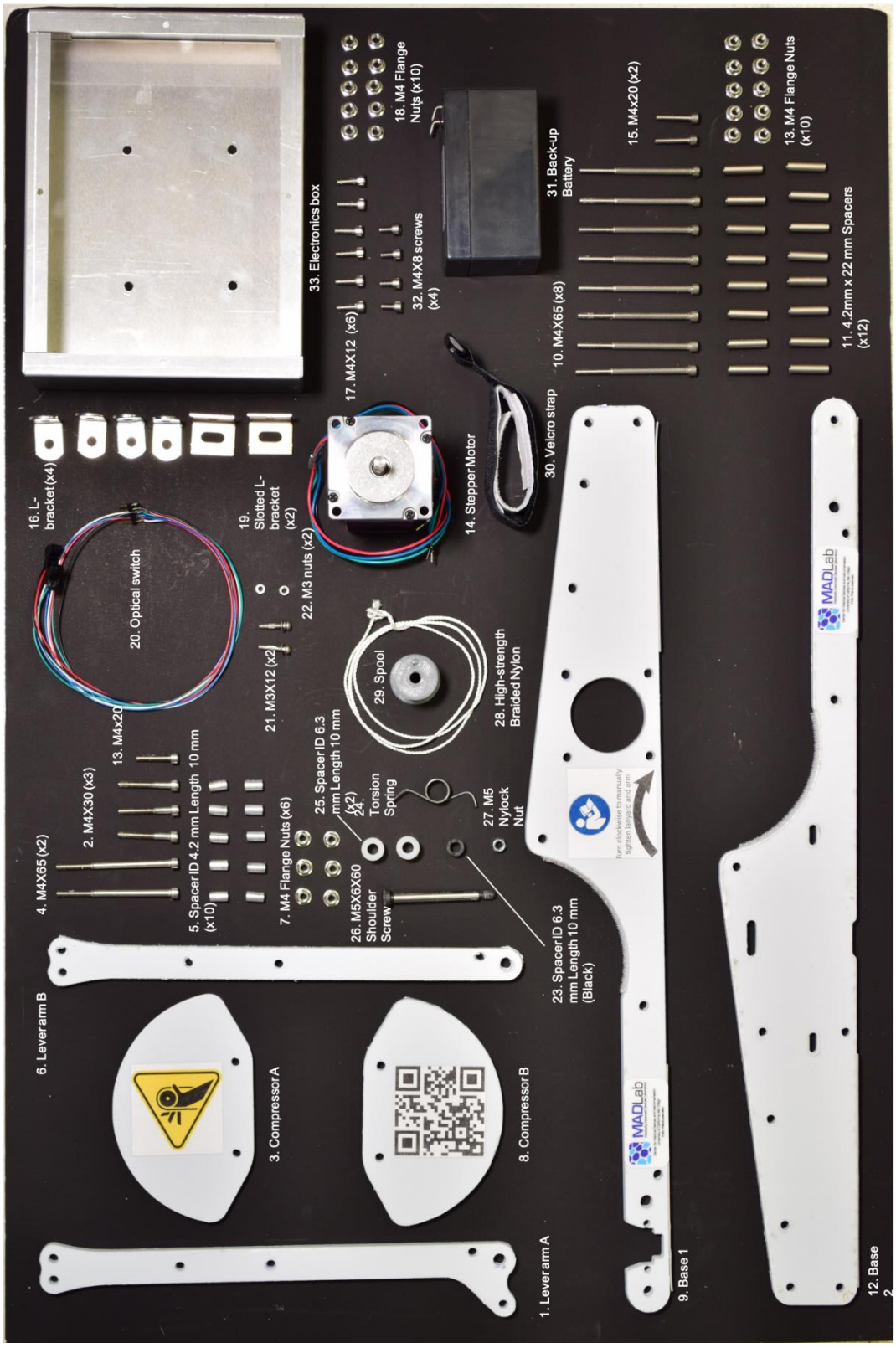

Figure 6: Components the MADVent Mark V. Self-inflating manual resuscitation bag, electronics box lid, PCB, and tubing are not shown.

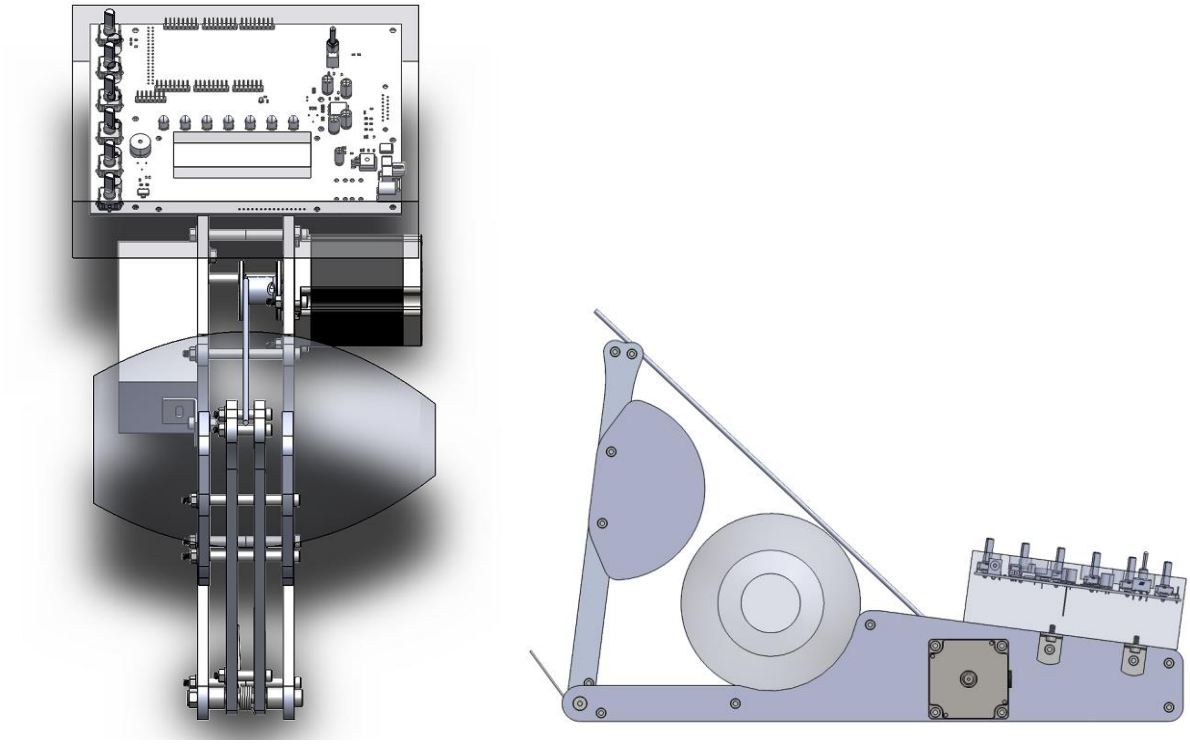

(a) (b)

Figure 7: SolidWorks rendering of the MADVent Mark V, with emphasized visibility of the pulley mechanism from (a) top-down and (b) side views.

The MADVent prototype frame components are laser cut from polyoxymethylene (acetal), but other materials may be used if polyoxymethylene is unavailable. Polycarbonate, which has shown to be durable against harsh disinfectants found in hospitals, is recommended as an alternate frame material. Note that polyoxymethylene can be laser cut in as few as 15 min., but other materials require more time and may be less desirable for rapid manufacturing.

3.1.2 Self-Inflating Manual Resuscitation Bag

Self-inflating manual resuscitation bags are FDA approved, well-documented, commonly found in hospitals, and inexpensive to purchase. These resuscitation bags have a preset range of deliverable tidal

volumes that enhance safety to the MADVent system. The resuscitation bags are also equipped with an attachable valve (PEEP Valve, Ambu Inc., MD, USA) that allows for easy application of PEEP with minimal additional dead space added to the system (Figure 8). The spring-loaded attachment, which connects to the resuscitation bag output functions by resisting the expiration of gas when the expiratory pressure becomes less than the PEEP setting.

Figure 8: Ambu® PEEP disposable valve. This valve has a range of 1.5 - 20 cm H2O, maintained by the internal spring. [59]

While unnecessary in many BMV use scenarios, the resuscitation bags also have additional connection points that enable oxygen administration and pressure monitoring for stable patients. This is particularly important for COVID-19 use scenarios, where increased physiological dead space reduces gas transfer and necessitates high FiO2 administration.

The resuscitation bag connects below the lever arm on a concave surface on the MADVent frame using a hook-and-loop connection (Velcro, United Kingdom) that allows for rapid resuscitation bag removal if a patient must be moved independently of the ventilator or if BMV is deemed necessary (Figure 9). While dead space is minimized by maintaining the resuscitation bag design, providers should also reduce the length of tubing between the resuscitation bag and the endotracheal tube to reduce dead space.

Incorporating a resuscitation bag into the MADVent design chosen due to proven reliability, simplicity of their design, and convenient integrated features. The choice of a standard resuscitation bag also provides a direct interface for standard ventilator circuit tubing compatible with bag valve masks, endotracheal tubes, tracheostomy tubes, and high efficiency particulate air (HEPA) filters.

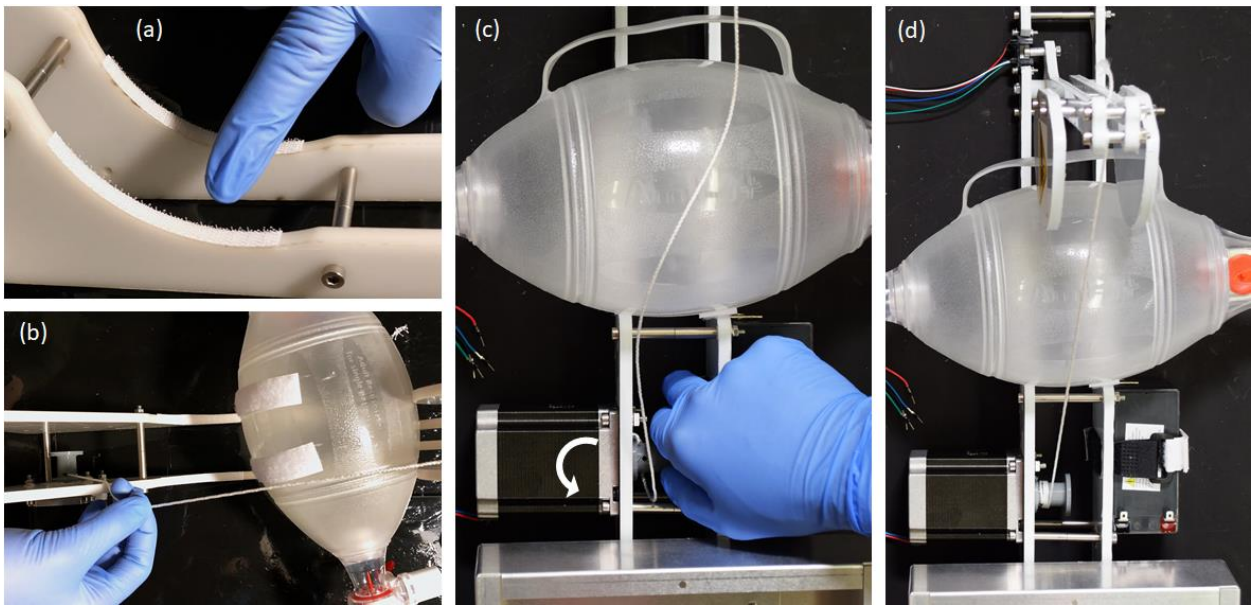

Figure 9: Incorporation of the self-inflating manual resuscitation bag into the MADVent Mark V design. Image reproduced from the MADVent Mark V Assembly Guide.

3.2 Pressure-Control

The choice to pressure-control the MADVent design reduces both cost and complexity. Pressure-control and volume-control devices require pressure or flow sensors, respectively, to monitor input values and report values to a feedback system. Flow sensors with adequate sensitivity are expensive and must perform instantaneous integrations to determine volume. Flow control can be preferable since input waveforms can be controlled, but in practice, this functionality only adds limited value in global emergencies. Differential pressure sensors are comparatively straightforward in design and less expensive to purchase. An inline Honeywell differential pressure-sensor was chosen for this device

(SSCMRRN060MDSA5, Honeywell Inc, NC, USA); two Bosch pressure sensor measured ambient and inline pressure in previous MADVent models (BMP180, Bosch Sensortec GmbH, Reutlingen, Germany).

3.3 Stepper Motor

The pulley mechanism is actuated by a stepper motor. Necessary torque for the system was determined and a stepper motor (QSH5718-76-28-189, Trinamic Motion Control GmbH, STATE, USA) exceeding the torque demand was selected for use in the MADVent.

The MADVent software has been developed around the Arduino Mega microcontroller (Arduino, STATE, USA). The main feature of the software is the pressure-control feedback loop that minimizes risk of volutrauma by maintaining pressure within acceptable levels and using a volume calculation as a secondary control. Although MADVent was not equipped with a flow sensor, a relationship between motor rotation and resuscitation bag compression was determined to estimate volume. The encoder (ECW1J-C24-BC0024L, Bourns Inc, CA, USA) counts the stepper motor's steps and applies them to the volume estimate equation. This estimate provides additional safety and ensures that predetermined volumes are not exceeded during ventilation. The derivation for the motor rotation volume calculation is appended Supplemental File 1.

3.4 Safety and Interface Features

The MADVent is equipped with several features that improve system safety and robustness. In addition to a standard 12VDC power supply that normally powers the unit, this ventilator includes a rechargeable back-up battery (BP1.2-12-T1, B Battery, China) that can power ventilation for up to 20 minutes after power source conversion. The MADVent additionally includes an optical switch (C14D32P-A3, CUI Devices, OR, USA) to ensure complete motion and resetting of the lever arm. Thermistors (2200/22SWH-100, Daburn Electronics, NJ, USA) have been attached to the motor and motor controller.

Though the MADVent does not have the full customizability of a high acuity commercial ventilator model, MADVent provides a series of controls and alarms to maximize quality of treatment and safety. The liquid crystal display (LCD) (LCD-14074, Sparkfun Electronics, CO, USA) and healthcare provider interface (Figure 10) allows users to monitor and control various parameters to best suit a patient's needs; these parameters and their ranges of operation are found in Table 3.

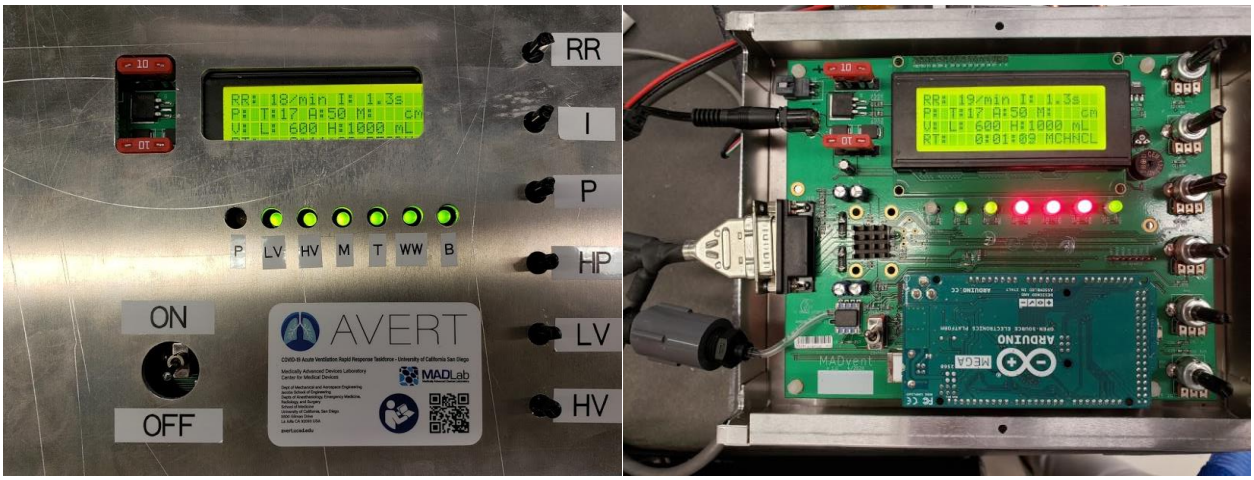

Figure 10: MADVent user interface and PCB. Users provide input using the on/off toggle switch and parameter adjustment potentiometers. Parameters and real-time pressure and time measurements can be viewed on the LCD screen. System alarm statuses are indicated by LEDs.

Table 3: Customizable MADVent Mark V parameters, their associated ranges of operation, and the increment of change for each parameter.

Parameter	Range of Operation	Increment
Respiratory rate	6 – 35 bpm	1 bpm
Positive inspiratory pressure (also called target pressure for this system)	10 – 35 cmH2O	1 cmH2O
Inspiratory time	1 – 3.0 s	0.1 s
High-pressure alarm threshold	30 – 60 cmH2O	1 cmH2O
Low-volume alarm threshold	200 – 1000 ml (must be set below high-volume alarm threshold)	20 ml
High-volume alarm threshold	200 – 1000 ml	20 ml
PEEP*	0 – 20 cmH2O	5 cmH2O

*PEEP can be adjusted using the PEEP valve built into the resuscitation bag. PEEP settings do not appear on the LCD user interface.

Each of these parameters, instantaneous pressure, total run time are displayed on the LCD. When each of the parameters are determined and appropriately adjusted, the ventilator can be initiated with the toggle switch.

The LCD also works with a series of light emitting diodes (LEDs) and a 92dB buzzer (CEM-1203(42), CUI Devices, OR, USA) to alert providers of seven hazardous ventilation conditions:

1. The high-pressure threshold is exceeded, or the pressure sensor is disconnected,
2. The low-volume threshold is not generated,
3. The high-volume threshold is exceeded,
4. Mechanical failure of the lever arm,
5. Overheating of the stepper motor or motor controller,
6. Back-up battery disconnection,
7. And wall power malfunction.

Adverse pressure or volume threshold events are triggered by the differential pressure sensor or encoder, respectively, and feedback mechanism will attempt to adjust the applied pressure to a safe level. Mechanical failures are initiated if the photo interrupter switch fails to trigger the optical sensor, indicating incomplete or failed motion of the lever arms. Temperature sensors are triggered if the thermistors register temperatures exceeding 65°C. The battery and wall power alarms will start if no connection is registered from the respective source.

3.5 Additional Details

The original MADVent Mark V prototype seen in Figure 5 has now been updated to include a printed circuit board (PCB) to consolidate electrical components, housing for the PCB with labeled casing, laser-cut acrylic housing for the entire ventilator meant to reduce pinching hazards, and updated code. The open-source design information includes product labeling, operating instructions, ventilator parts and detailed assembly procedure, and technical description documents. A complete part list and assembly manual are appended Supplemental File 1.

4 VALIDATION

The objective of this section is to describe the equipment and methods used to validate the MADVent.

4.1 EQUIPMENT

Flow and pressure were collected using the VVK100-SYS Ventilator Validation Kit (BIOPAC Systems, Inc., CA, USA), equipped with a 16-channel data acquisition system (MP160WS/W), laminar flow transducer and amplifier (TSD157B-MRI-01), and differential pressure transducer with amplifier (TSD160D) (BIOPAC Systems, Inc., CA, USA). Acq*Knowledge* software (Version 5.0, BIOPAC Systems, Inc., CA, USA) was to interface with the data collection system and perform any necessary post-processing. The flow and pressure transducers were connected in series between the MADVent resuscitation bag and the test lungs. Prior to data collection, the system was calibrated using a 3-liter calibration syringe (BIOPAC Systems, Inc., CA, USA).

Benchtop tests were performed using a mechanical lung simulator (Dual Adult Test Lung, Michigan Instruments, MI, USA). Ex-vivo tests were performed using a porcine lung due to the close resemblance of porcine and human respiratory anatomies. Prior to testing, the porcine lung (Nasco Healthcare Inc., NY, USA) was stored in 25% propylene glycol solution to preserve the tissue's mechanical properties. A handheld infrared temperature gun (Lasergrip 774 Infrared Thermometer, Etekcity, CA, USA) was used to collect surface temperature data.

4.2 RISK MITIGATION

ISO standard 14971:2019 (International Standards Organization, 2019a) which requires evaluation of risks for medical devices and clinical procedures and implementation of a risk management system. Risks for the system were brainstormed and evaluated using a risk acceptability matrix; methods to reduce or eliminate risks were implemented for those that were severe or common.

Use of an alarm system substantially mitigated risk. The alarms, detailed in 3.4, were tested by artificially imposing risk conditions onto the system during operation. All simulation methods were applied during a trial, after equilibrium had been established. These tests were run using a respiratory rate of 13 bpm, PEEP of 15 cmH2O, and lung compliance of 0.03 L/cmH2O. High-volume threshold was tested by decreasing PEEP from 15 to 5 cmH2O. Low-volume threshold was tested by increasing PEEP from 15 to 17 cmH2O. Adjusting PEEP for volume threshold testing is effective since delivered volume changes with changes in the difference between baseline and target pressures. High-pressure threshold was tested by temporarily adding a kink to the circuit tubing to simulate a cough.

4.3 Adverse Condition Study

An adverse ventilation study was performed in accordance with ISO 80601-2-80:2018, Table 201.105. For this set of test trials, the mechanical lung simulator was secured to the ventilator via circuit tubing. This study assumed identical compliance and resistance levels in both the left and right lungs, allowing use of single lung rather than dual lung settings. The parameters for each trial, as defined by the relevant TVs in Table 201.105, test the ventilator under extreme operating conditions. The parameters are listed in Table 4, with excluding the 1s inspiration time used for all trials. TV was also calculated for each trial, using Equation 18, which is a rearrangement of Equation 12.

$$V_T = C_{Dynamic}(PIP - PEEP) \tag{18}$$

Table 4: Relevant parameters used during the adverse conditions study. Inspiration time was set to 1s for all trials.

Trial	Parameters					
	Intended TV (mL)	Compliance (L/cmH2O)	Resistance (hPa/L/s)	RR (bpm)	PIP (cmH2O)	PEEP (cmH2O)
1	500	0.05	5	20	10	5
2	500	0.05	20	12	15	10
3	500	0.02	5	20	25	5
4	500	0.02	20	20	25	10
5	500	0.02	20	20	15	5
6	500	0.02	50	12	25	10
7	300	0.01	50	20	30	5
8	300	0.01	10	20	25	10

4.4 24-HOUR STUDY

A 24-hour validation study was performed in accordance with ISO 80601-2-80:2018 and AAMI CR503:2020. For this study, the mechanical lung simulator was secured to the ventilator via circuit tubing. This study assumed identical compliance and resistance levels in both the left and right lungs, allowing use of single lung rather than dual lungs settings. The ventilator was turned on and left to run continuously for 24-hours using a RR of 30 bpm, PIP of 40 cmH2O, PEEP of 4 cmH2O, lung compliance of 0.01 L/cmH2O, and lung resistance of 50 hPa/L/s. These parameters include the maximum possible RR and TV for the MADVent as indicated by the instructions for use. Flow and pressure data were collected. A live webcam stream was enabled so ventilator function could be monitored remotely.

4.5 EX-VIVO STUDY

A porcine lung was attached to the end of the ventilator via circuit tubing and was laid flat on a counter to minimize abnormal loading on the tracheobronchial tree. The tubing was shortened as much as possible to limit additional dead space in the system. The porcine lung was initially inflated using the ventilator on low PEEP (5 cmH2O) and a moderate target pressure (21 cmH2O) to precondition the tissue after stagnation in the preserving solution. Flow and pressure data from this period of cycling the lung using the ventilator were not recorded, however, video recordings were taken. “Dead” areas of the lung with minimal inflation were massaged in conjunction with manual compression of the resuscitator bag to encourage greater tissue recruitment. A physician approved the state of the porcine lung prior proceeding to recorded trials.

After preconditioning, 9 ex-vivo trials were completed using the parameters described in Table 5. These trials were video-taped, and flow and pressure data were recorded.

Table 5. Ex-vivo trial parameters.

Trial	**Parameters**			
	Inspiration Time (s)	RR (bpm)	PIP (cmH2O)	PEEP (cmH2O)
1	1	12	25	10
2	1	12	20	10
3	1	12	25	10
4	1	12	25	10
5	1.3	12	25	10
6	1	12	30	10
7	1.6	12	30	10
8	1.3	12	30	15
9	1.3	12	30	15

4.6 Active Cooling Assessment

A comparison study was conducted to assess the impact of active cooling on suspected overheating of the MADVent. Small fans (AI-MPF80A2, AC Infinity Inc., CA, USA) were placed behind the motor and PCB; the lid of the electronics box was removed to allow direct airflow across the PCB. Temperature data was collected from the heat sink, an arbitrary location on the PCB, and the power source on the Arduino at selected timepoints. Data was collected after allowing the ventilator to idle for one minute and after running the ventilator for 5 minutes continuously. The continuous collection point was repeated for a total of 3 trials. These trials were completed with and without active cooling.

4.7 Post-Processing and Statistics

Acq*Knowledge* software was used to post-process pressure and flow data. Differential pressure data output directly from the data acquisition system did not require additional processing. Raw flow data were transformed using a series of calculation-based channels in the software. The calculations performed at each time point to refine flow data and yield volume data are shown in Figure 11.

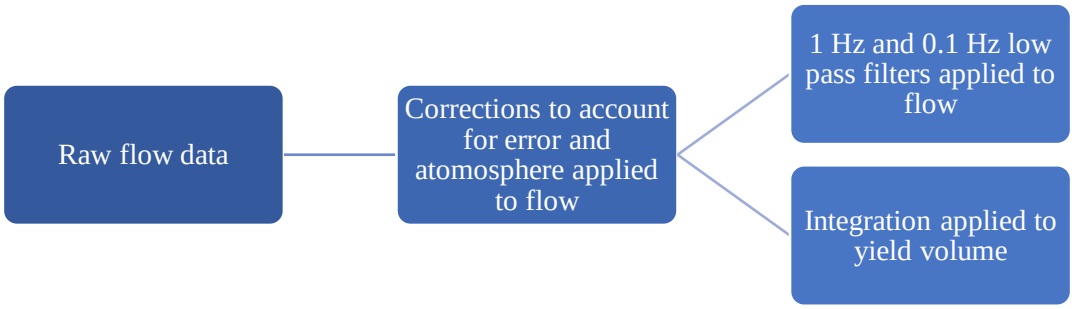

Figure 11: Flow chart outlining the post-processing steps used to yield final flow and volume data.

Acq*Knowledge* data were exported to MATLAB (MathWorks, MA, USA). Dynamic compliance of the porcine lung was determined by dividing the tidal volume by the difference in pressure at the beginning and end of inspiration, as described by Equation 12. Compliance calculations were performed

on three cycles each from three different trials with identical parameters apart from their distinct target pressures.

Two-way repeated measures, ANOVA and post-hoc Tukey tests were conducted to analyze the impact of having of active cooling and the area of cooling (Arduino power source, PCB heat sink, PCB open space) on cooling efficacy. Significance was defined as $p < 0.05$. Statistics were performed in Minitab (Version 19.1, Minitab Inc., PA, USA).

5 RESULTS

The objective of this section is to describe the results of the validation tests performed on the MADVent.

5.1 RISK MITIGATION

Output from volume and pressure threshold testing are seen in Figure 12. Pressure-driven tests demonstrate functionality of the high-volume threshold alarm, low-volume threshold alarm, and high-pressure threshold alarm.

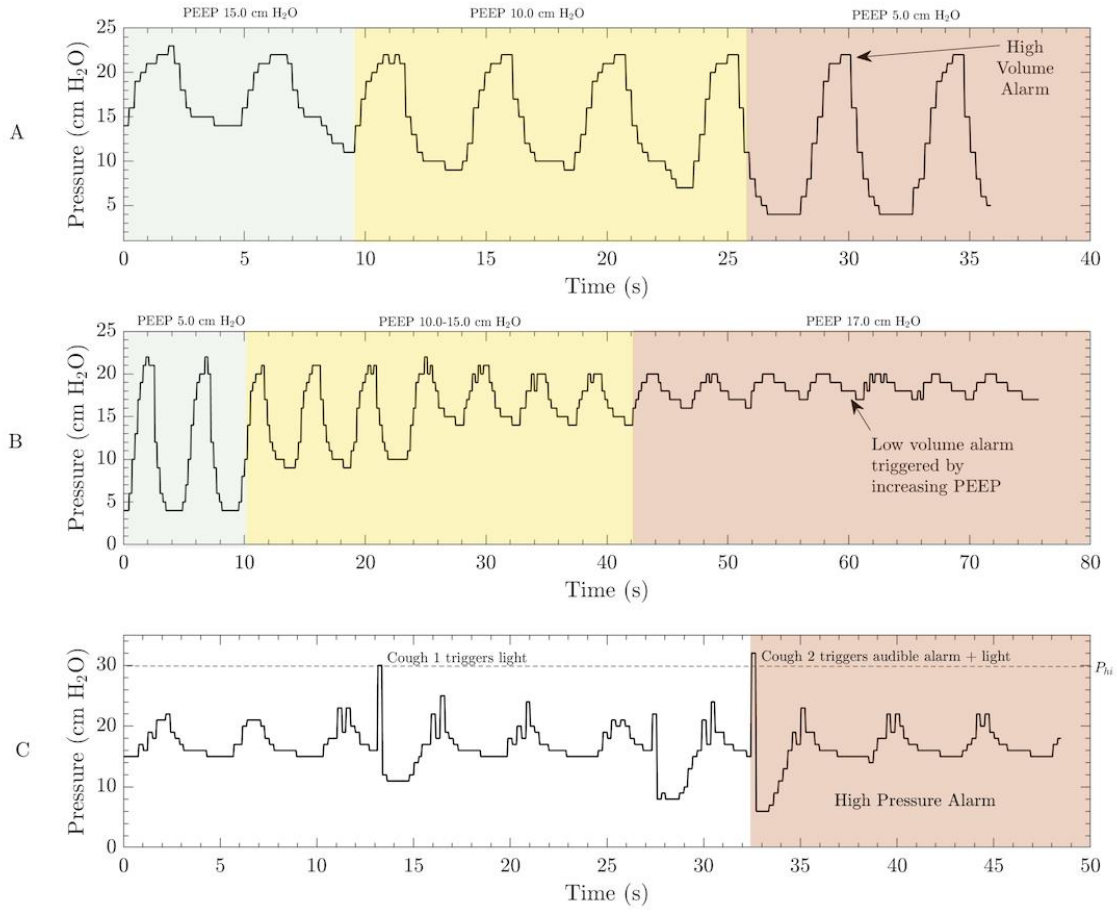

Figure 12: Results from (a) high-volume threshold alarm, (b) low-volume alarm threshold, and (c) high-pressure alarm threshold testing. High- and low-volume thresholds were artificially met by adjusting PEEP during the trial. High-pressure thresholds were met by adding kinks to the circuit tubing.

5.2 Adverse Condition Study

A sample representative of the twelve adverse clinical conditions is shown in Figure 16. This trial was the result of the first applicable condition set in ISO80601-2-80:2018, Table 201.105, where the intended TV was 500 mL, compliance was 0.05 L/cmH2O, resistance was 5 hPa/L/s, RR was 20 bpm, PIP was 10 cmH2O, and PEEP was 5 cmH2O. Other trial results can be found in Supplemental File 1. None of these trials exceeded pressure or volume thresholds or showed other signs of malfunction. Intended TV, measured TV, and associated Trial number are listed in Table 6. Intended and measured TV did not align, but measured TV and calculated TV (Equation 18) were similar.

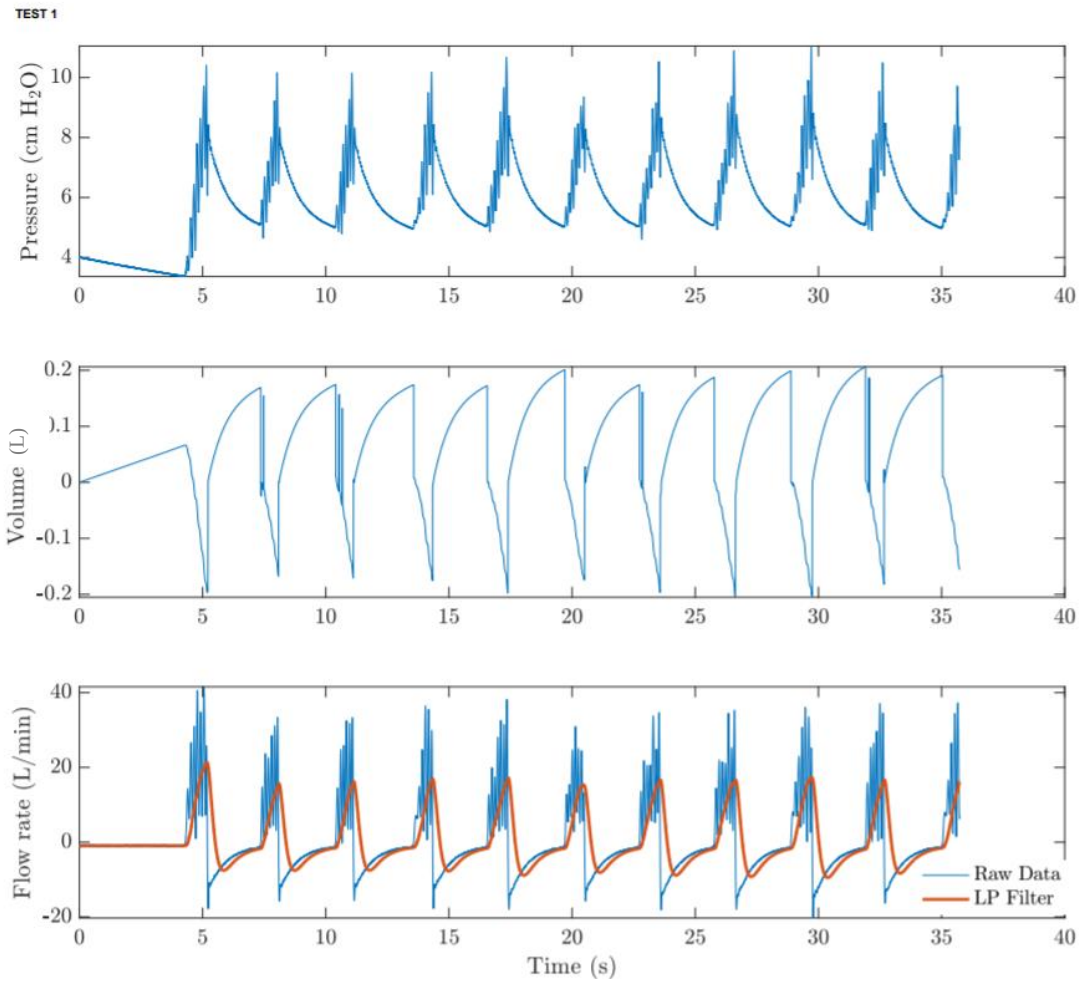

Figure 13: The first of the 12 adverse clinical conditions applicable to the MADVent, as defined ISO 80601-2-80:2018, Table 201.105. The following parameters were used: compliance of 0.05 L/cmH2O, resistance of 5 hPa/L/s, RR of 20 bpm, PIP of 10 cmH2O, and PEEP of 5 cmH2O.

Table 6: Comparison of intended, measured, and calculated TV for relevant adverse clinical conditions as described by ISO 80601-2-80:2018, Table 201.105.

Trial	Intended TV (mL)	Measured TV (mL)	Calculated TV (mL)
1	500	236	250
2	500	212	250
3	500	384	400
4	500	292	300
5	500	166	200
6	500	187	300
7	300	203	250
8	300	167	150

5.3 24-HOUR STUDY

Results from the first 60 seconds beginning and ending 60 seconds of the 24-hour study are seen in Figure 14 and Figure 15, respectively. Comparison of these figures demonstrates consistency in ventilator function throughout the 24 hours.

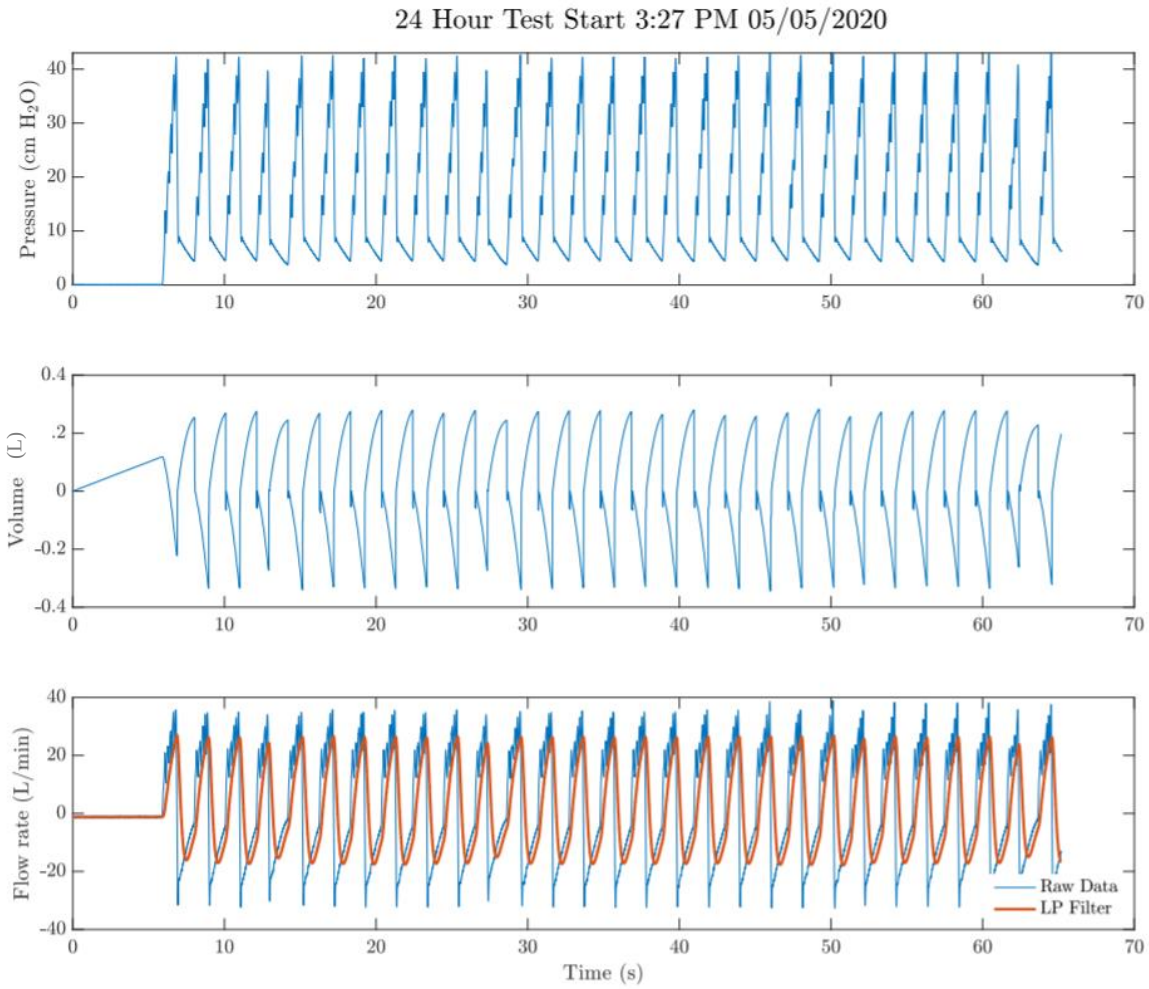

Figure 14: 60 second data sample from the beginning of the 24-hour study. The following parameters were applied: RR of 30 bpm, PIP of 40 cmH2O, PEEP of 4 cmH2O, lung compliance of 0.01 L/cmH2O, and lung resistance of 50 hPa/L/s.

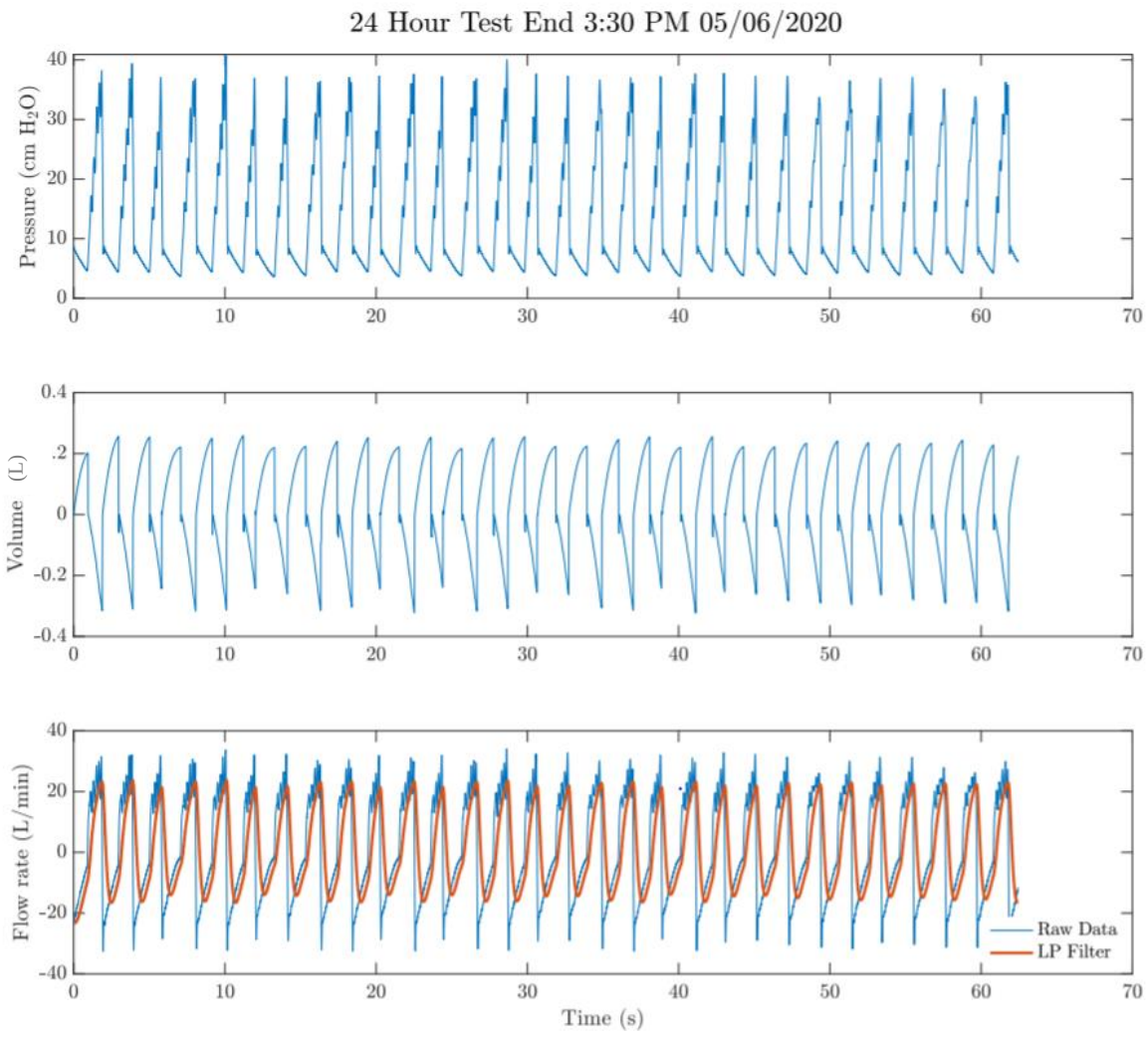

Figure 15: 60 second data sample from the end of the 24-hour study. The following parameters were applied: RR of 30 bpm, PIP of 40 cmH2O, PEEP of 4 cmH2O, lung compliance of 0.01 L/cmH2O, and lung resistance of 50 hPa/L/s.

5.4 Ex-Vivo Study

Output from the ex-vivo trials follow expected waveforms patterns. A sample representative, Trial 4, is shown in Figure 16. This figure includes 60 seconds of data from the approximately 500 second trial. A zoomed in 10 second snapshot of this data is found in Figure 17. Other trial results can be found in Supplemental File 1. Video footage of this trial can also be found in Supplemental File 2.

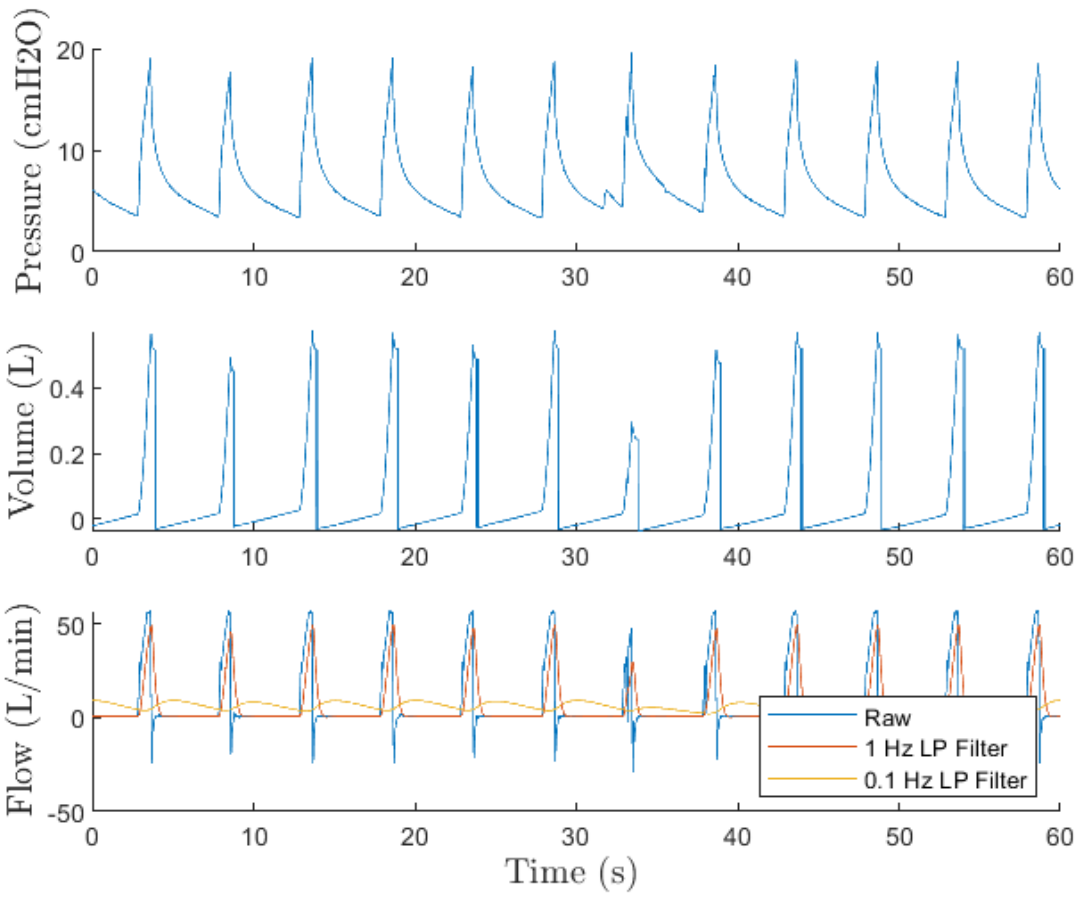

Figure 16: Example waveforms developed during the ex-vivo study. This trial (Trial 4) used the following parameters: inspiration time of 1s, RR of 12bpm, PIP target of 25 cmH2O, and PEEP of 10 cmH2O. This figure shows a 60 second excerpt from trial 4.

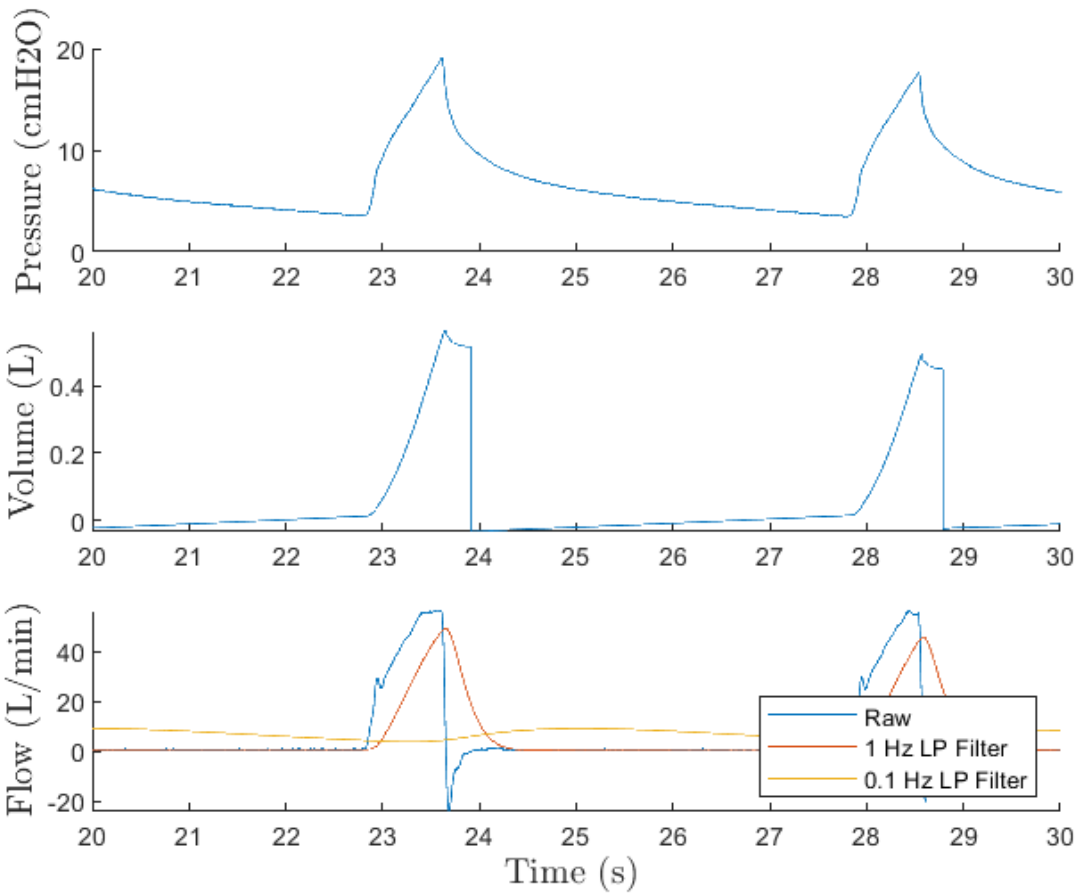

Figure 17: Example waveforms developed during the ex-vivo study. This trial (Trial 4) used the following parameters: inspiration time of 1s, RR of 12 bpm, PIP target of 25 cmH2O, and PEEP of 10 cmH2O. This figure shows a 10 second excerpt from trial 4 to allow for greater resolution.

Measured TV, PIP, and PEEP from representative cycles in trials 2, 4, and 7 are shown in **Error! Not a valid bookmark self-reference.**. The calculated dynamic compliance values for each cycle and the averaged value for all cycles are also shown in **Error! Not a valid bookmark self-reference.**. Dynamic compliance was determined to be 0.037 L/cmH2O for the porcine lung used in all ex-vivo trials. Dynamic compliance appears to increase as target PIP increases.

Table 7: Compliance of the porcine lung was determined using Equation 12. The measured TV, PIP, and PEEP were taken from three representative cycles each from three separate ex-vivo trials. These values were used to calculate dynamic compliance and were then averaged. Based on these calculations, the dynamic compliance of the porcine lung was 0.037 L/cmH2O. The three trials (2, 4, 7) had different target PIP, ranging from 20 to 30 cmH2O, but had the same remaining parameters. For these trials, an inspiration time of 1 s, RR of 12 bpm, and PEEP of 10 cmH2O were used.

Trial	**TV (L)**	**PIP (cmH2O)**	**PEEP (cmH2O)**	**Dynamic Compliance (L/cmH2O)**
Trial 2 (Target PIP = 20 cmH2O)	0.351	16.839	3.172	0.026
	0.297	15.788	3.376	0.024
	0.356	16.077	3.454	0.028
Trial 4 (Target PIP = 25 cmH2O)	0.572	20.050	3.625	0.035
	0.555	19.348	3.817	0.036
	0.558	19.019	3.585	0.036
Trial 7 (Target PIP = 30 cmH2O)	0.789	21.147	4.026	0.046
	0.781	20.346	4.006	0.048
	0.794	19.499	4.000	0.051
			Average:	**0.037**

5.5 Active Cooling Study

Temperature data procured during the active cooling study are found in Table 7. Two of the three running ventilator trials were aborted partway through the trial for the no active cooling group due to failure of the ventilator.

Table 8: Temperature data collected in the active cooling comparison study. Temperatures were collected from the Arduino, PCB heat sink, and PCB open space at various time points.

	Ventilator Action	Temperature (°C)		
		Arduino Power Unit	PCB – Heat Sink	PCB – Open Space
	Off	23	23	23
Active Cooling	Standing idle for 1 min	40	24	25
	Running for 5 min	30	24	30
	Running for 5 min	51	28	31
	Running for 5 min	47	29	30
No Active Cooling	Standing idle for 1 min	43	30	24
	Running for 5 min	62	35	43
	Running for 5 min*	72	38	52
	Running for 5 min*	73	32	45

* Trials failed and did not complete 5 continuous minutes of ventilation. Temperature was recorded after trial failure.

Significant differences were found between active cooling and no active cooling groups for the PCB – Heat Sink ($p < 0.039$) and PCB – Open Space ($p < 0.049$) locations. The ventilator's idling and running temperatures were additionally significantly at the PCB – Open Space location ($p < 0.007$). When the active/no active cooling and idle/running status were made cross-factors, significant differences were found between no active cooling while the ventilator was running and all other configurations ($p < 0.034$). These results suggest that ventilator failures are attributed to overheating of the general PCB rather than a specific area, and that overheating is not due to a failure or inadequacy of the currently installed heat sink. ANOVA and post-hoc Tukey test results are summarized in Appendix A.

6 DISCUSSION

The objective of this section is to discuss the implications of data shown in the results, the limitations of the study, and the next steps for this project.

6.1 MADVENT DESIGN

The MADVent design is developed to be low-cost and easily sourced, while also being safe and effective. The design established here uses a mixture of off-the-shelf and easily accessible pieces such as a self-inflating resuscitation bag to ensure that costs remain low. The resuscitation bag had the additional benefits of being FDA approved, rated to deliver a safe range of tidal volumes, and compatibility with PEEP valves and standard tubing connectors. The MADVent also employed a novel pulley mechanism that allowed for efficient torque conversion. The stepper motor utilized in this design allowed for an approximate calculation of delivered volume despite the design being a pressure-controlled system.

The alarm functionalities of the MADVent are particularly unique for low-cost emergency ventilators. The money saved using the lanyard and pulley design mitigated the need for an in-line flow sensor that are necessary for many low-cost ventilator designs. These flow sensors often allow the user to pick the delivery waveform, but this is not an essential modality especially considering the lack of evidence that specific waveforms optimize patient care. Contrarily, incorporated visible and audible alarms may be lifesaving for a patient who has encountered a ventilator malfunction.

The MADVent design totals $233.95 (Supplemental File 1). This cost considerably undercuts the cost of commercial ventilators and is competitively priced as a low-cost ventilator. The choice to use pressure-controlled ventilation allowed for purchase and implementation of a differential pressure sensor as opposed to a flow sensor, which cost about $10 and $150 per unit, respectively. The design also has fewer parts that would need to be replaced in the occasion of excessive wear, further reducing lifetime costs.

The MADVent design does have a few limitations. PCB overheating was determined to be a significant issue in the MADVent that will require correction in future models. Interestingly, the existing heat sink attached to the PCB seemed to be performing adequately but was simply not robust enough to regulate temperature across the whole board. The addition of an active cooling component to the PCB was shown to significantly improve the ventilator function and should be added as a permanent feature of the PCB in the future. The occasional skipped steps by the motor may also be attributable to overheating. This symptom should be reevaluated after an additional cooling component is added.

The PCB differential pressure sensor was observed to output values that were a few cmH2O greater than detected by the benchmark MP160 differential pressure sensor. The differences between values are minimal and thus do not impede the overall function of the pressure-control feedback loop, but should be noted as a weakness in sensitivity.

The MADVent design currently does not feature any notable housing. The absence of housing exposes users to hazardous pinch-points around the lever arm that will require mitigation prior to an FDA submission. A robust housing would be beneficial to reduce user risk, reduce damage to the ventilator, and optimize portability of the ventilator. The patient transportation application of this ventilator requires enhanced portability functions which could be solved with a clever housing design. A version of the MADVent includes redesigned base pieces that with large hooks that can be used to hang the ventilator in emergency transport vehicles or gurneys. While the pulley design of this ventilator configuration remains identical to the MADVent Mark V, further testing must be done to ensure that a suspended orientation does not impede ventilation functionalities.

6.2 Mechanical Lung Simulator Studies

The 12 adverse side effects tests affirm the safe operating range of the MADVent. Combined with the alarm system, healthcare providers can make informed decisions about how to best set their patient's ventilation settings. The addition of a 24-hour long test additionally builds confidence in the system. Not

only can the ventilator work at max power, but the ventilator can also maintain these standards for long periods of time without compromising quality of care.

The waveforms output by each of the mechanical lung simulator studies are similar in shape, despite the large variation in parameters. The pressure curves do not fit well with either traditional volume-controlled or pressure-controlled waveforms. This could be partially due to the large target PIP values used in testing ventilator and short I:E times used during testing.

The volume waveforms are unique in these tests as well. While the inspiratory half of the curves have excellent agreement with pressure-controlled volume curves, the expiratory half of the curve crosses the x-axis and has repeated negative values. The volume should never be negative in PPV, indicating an error in either the ventilator or data collection system. The latter seems more likely since the volume is dependent on a unique integration of the flow in the Acq*Knowledge* software. This integration lacks an integration constant and instead resets the volume at zero whenever certain voltage thresholds are reached in the raw voltage data. Two almost identical integrals are calculated, with the first assuming a positive slope with the reset incidence and the second assuming a negative slope with the reset incidence. An IF statement is then used to determine which of these values should be used at each time point. If there was any error in data collection, then the error may be exaggerated in the volume waveform.

The flow waveform appears to be standard regarding positive pressure controls. A distinct positive inspiratory slope peaks at a maximum value, then decelerates before becoming negative. These curves lack the plateau phase often found in volume-controlled flows.

The mechanical lung simulator is commonly employed to validate commercial ventilators; however, there are limitations to this form of testing. While the elastomer bellows and spring-controlled compliance do simulate nonlinear, parabolic lung characteristics, the anisotropic, non-homogeneous nature of tissue cannot be completely modeled. These issues are addressed by the ex-vivo portion of this validation. The test set-up additionally included an excess of dead space in order to incorporate the BIOPAC differential pressure and flow sensors in line with the ventilator and mechanical lung simulator.

6.3 EX-VIVO STUDY

Although MADVent safety features are largely validated using the mechanical lung model, it is important for ventilators to be tested on mammalian lung prior to receiving any approvals. Human life, particularly lives that are already at risk from injury or disease, should be treated with precaution and medical devices should be evaluated thoroughly before advancing to in-person use. These tests allow for observation and understanding of how non-homogeneous, anisotropic material properties interact with the device. These properties vary not only throughout the tissue and respiratory structures, but also throughout their range of expansion and contraction. While mechanical and theoretical systems can attempt to model this, they cannot fully encompass the complex function at a macro level. The MADVent ex-vivo trials use porcine lungs due to their close similarities to human respiratory anatomy and physiology.

It is also pertinent to test ex-vivo models before progressing to in-vivo models. While porcine lungs like those used in the MADVent ex-vivo study can be sourced from slaughterhouses where large organs may otherwise go to waste, an in-vivo model usually requires sedation, injury, or the eventual sacrifice of the animal. The sacrificial process can be particularly involved for large mammals.

Upon analysis, the waveforms output in the ex-vivo trials are consistent with those expected from a pressure-controlled device. The pressure waveform features a rapidly rising curve that peaks, and the rapidly declines. This may seem more indicative of volume control, however, the extremely short, 1s inspiratory time used in ex-vivo trial 4 disallows the flat plateau that would normally occur. As soon as PIP is reached, expiration begins; for this trial, the I:E is very uneven, with expiration time being approximately 4s to the 1s of inspiration.

The small I:E similarly alters the shape of the volume and flow waveforms. The volume slope rapidly rises because of the short inspiration time, and then even more rapidly decreases since the expiration resistance is so small. There is evidence of a leak in the tissue. The brief, slower decrease in volume could be attributed to air leaking out through holes in the lungs prior to complete release of pressure; this notion is supported by visual observations of small holes in the pleural layer of the lung.

The flow waveform similarly fits expectations for a pressure-controlled ventilator. The curve has a defined peak as opposed to a plateau. Like the pressure and volume curves, the decrease of flow is particularly steep, a quality that may be attributable to the I:E.

While the nonzero pressure baseline indicates that PEEP is applied to the system, the PEEP values measured notably vary from the intended values listed in the parameters. Intended PEEP of 10 cmH2O yielded measured values below 5 cmH2O. Low PEEP is often seen as preferable for ventilated patients, except for ARDS victims who are known to benefit from higher PEEP strategies.

The porcine lung was sourced from a slaughterhouse and may have incurred rips or air leaks causing abnormal, incomplete, or uneven inflation. As noted previously, there were visible holes in the pleural membrane that allowed leaking in the system. Upon review of video recordings, there was also a large portion of the lung that would not inflate or would only inflate minimally. It is likely that this region of the lung had atelectasis that could not be overcome during the preconditioning process. The visible damage of the lung was reflected in the low calculated dynamic compliance of 0.037 L/cmH2O. While diseased and damage lungs were not considered ideal for this ex-vivo study, the MADVent has now been shown to effectively deliver ventilation to lungs in dire condition. This is encouraging since patients requiring mechanical ventilation often have lungs that are similarly deteriorated.

While ex-vivo studies are an essential step of showing efficacy in ventilating biological material, the porcine lung is not a completely representative model of a living organ. Essential respiratory features including the surface tension generated by alveolar fluid and the counterbalancing production of surfactant are not viable in fixated tissue. Due to a lack of pleural sac support, the porcine lung was also ventilated while lying flat on a counter. This orientation increases the resistance that must be overcome during ventilation. Ex-vivo models additionally lack the gas exchange functionality of a living lung, preventing evaluation of oxygen delivery effectiveness. Future studies should evaluate ventilator function using an in-vivo model such as a sedated pig.

6.4 Future Considerations

The purposes of these tests are to secure FDA approval. Following an in-vivo trial, the immediate next step for MADVent is application for EUA or a 510k submission. EUA would allow for use in US hospital and emergency scenarios, and would predicate similar clearances from European Union regulatory bodies. The 510k process is more robust and a successful submission would allow for wider range of approved use.

7 CONCLUSION

Ventilator shortages have long been associated with mass casualty events at local and global levels, with the COVID-19 pandemic being the most recent. Low-cost, easily sourced, and easily assembled ventilator designs are essential to filling this void during crisis times. The MADVent is a single-mode continuous, mandatory, pressure-controlled, time-terminated device that has been developed to meet both these emergency use needs and serve as an alternative portable ventilator for use in low-income countries and for temporarily treating patients in transit.

The hypothesis for this study was that the proposed MADVent Mark V design could successfully inflate tissue for sustained periods, with waveforms that are verifiably safe and effective according to the regulatory bodies and standards for medical devices. The MADVent was designed with these standards in mind, enabling the innovative novel use of pulley mechanisms for torque conversion and volume approximations without a flow sensor. Because costs were minimized in the overall mechanistic design, the addition of life support features and alarms were able to be included. These features make the MADVent more safe and more robust than other known low-cost ventilators.

The validation studies assessing the qualities of these alarms and the effectiveness of the ventilator at extreme clinical conditions and durations yielded waveforms demonstrating that MADVent can be used reliably in a variety of scenarios. In this series of tests on the mechanical lung simulator and porcine lung, the MADVent affirmed the hypothesis and was proven to administer safe, effective, and sustained ventilation and also ventilation to porcine tissue in accordance with ISO, AAMI, and FDA standards. While there are limitations to these experiments, this data collectively indicates that MADVent can provide life-saving ventilation therapy for human patients and should proceed to in-vivo trials and subsequently be submitted to the FDA through the 510k process.

APPENDIX

A. STATISTICS

WORKSHEET 1

General Linear Model: Arduino versus Active Cooling, Status

Method

Factor coding (-1, 0, +1)

Factor Information

Factor	Type	Levels	Values
Active Cooling	Fixed	2	N, Y
Status	Fixed	2	Idle, Run

Analysis of Variance

Source	DF	Adj SS	Adj MS	F-Value	P-Value
Active Cooling	1	322.7	322.67	4.00	0.116
Status	1	308.2	308.17	3.82	0.122
Active Cooling*Status	1	204.2	204.17	2.53	0.187
Error	4	322.7	80.67		
Total	7	1675.5			

Model Summary

S	R-sq	R-sq(adj)	R-sq(pred)
8.98146	80.74%	66.30%	*

Coefficients

Term	Coef	SE Coef	T-Value	P-Value	VIF
Constant	48.67	3.67	13.27	0.000	
Active Cooling					
N	7.33	3.67	2.00	0.116	1.33
Status					
Idle	-7.17	3.67	-1.95	0.122	1.00
Active Cooling*Status					
N Idle	-5.83	3.67	-1.59	0.187	1.33

Regression Equation

Arduino = 48.67 + 7.33 Active Cooling_N - 7.33 Active Cooling_Y - 7.17 Status_Idle
+ 7.17 Status_Run - 5.83 Active Cooling*Status_N Idle
+ 5.83 Active Cooling*Status_N Run + 5.83 Active Cooling*Status_Y Idle
- 5.83 Active Cooling*Status_Y Run

Fits and Diagnostics for Unusual Observations

Obs	Arduino	Fit	Resid	Std Resid	
1	40.00	40.00	0.00		* X
5	43.00	43.00	0.00		* X

X Unusual X

WORKSHEET 1

General Linear Model: PCB - Heat Sink versus Active Cooling, Status

Method

Factor coding (-1, 0, +1)

Factor Information

Factor	Type	Levels	Values
Active Cooling	Fixed	2	N, Y
Status	Fixed	2	Idle, Run

Analysis of Variance

Source	DF	Adj SS	Adj MS	F-Value	P-Value
Active Cooling	1	73.500	73.500	9.19	0.039
Status	1	24.000	24.000	3.00	0.158
Active Cooling*Status	1	1.500	1.500	0.19	0.687
Error	4	32.000	8.000		
Total	7	170.000			

Model Summary

S	R-sq	R-sq(adj)	R-sq(pred)
2.82843	81.18%	67.06%	*

Coefficients

Term	Coef	SE Coef	T-Value	P-Value	VIF
Constant	29.00	1.15	25.11	0.000	
Active Cooling					
N	3.50	1.15	3.03	0.039	1.33
Status					
Idle	-2.00	1.15	-1.73	0.158	1.00
Active Cooling*Status					
N Idle	-0.50	1.15	-0.43	0.687	1.33

Regression Equation

PCB - Heat Sink = 29.00 + 3.50 Active Cooling_N - 3.50 Active Cooling_Y - 2.00 Status_Idle
+ 2.00 Status_Run - 0.50 Active Cooling*Status_N Idle
+ 0.50 Active Cooling*Status_N Run + 0.50 Active Cooling*Status_Y Idle
- 0.50 Active Cooling*Status_Y Run

Fits and Diagnostics for Unusual Observations

Obs	PCB - Heat Sink	Fit	Resid	Std Resid	
1	24.00	24.00	0.00		* X
5	30.00	30.00	0.00		* X

X Unusual X

WORKSHEET 1

General Linear Model: PCB - Open Space versus Active Cooling, Status

Method

Factor coding (-1, 0, +1)

Factor Information

Factor	Type	Levels	Values
Active Cooling	Fixed	2	N, Y
Status	Fixed	2	Idle, Run

Analysis of Variance

Source	DF	Adj SS	Adj MS	F-Value	P-Value
Active Cooling	1	88.17	88.17	7.78	0.049
Status	1	294.00	294.00	25.94	0.007
Active Cooling*Status	1	112.67	112.67	9.94	0.034
Error	4	45.33	11.33		
Total	7	740.00			

Model Summary

S	R-sq	R-sq(adj)	R-sq(pred)
3.36650	93.87%	89.28%	*

Coefficients

Term	Coef	SE Coef	T-Value	P-Value	VIF
Constant	31.50	1.37	22.92	0.000	
Active Cooling					
N	3.83	1.37	2.79	0.049	1.33
Status					
Idle	-7.00	1.37	-5.09	0.007	1.00
Active Cooling*Status					
N Idle	-4.33	1.37	-3.15	0.034	1.33

Regression Equation

PCB - Open Space = 31.50 + 3.83 Active Cooling_N - 3.83 Active Cooling_Y - 7.00 Status_Idle
+ 7.00 Status_Run - 4.33 Active Cooling*Status_N Idle
+ 4.33 Active Cooling*Status_N Run + 4.33 Active Cooling*Status_Y Idle
- 4.33 Active Cooling*Status_Y Run

Fits and Diagnostics for Unusual Observations

Obs	PCB - Open Space	Fit	Resid	Std Resid	
1	25.00	25.00	-0.00		* X
5	24.00	24.00	-0.00		* X

X Unusual X

WORKSHEET 1

Comparisons for Arduino

Tukey Pairwise Comparisons: Active Cooling

Grouping Information Using the Tukey Method and 95% Confidence

Active Cooling	N	Mean	Grouping
N	4	56.0000	A
Y	4	41.3333	A

Means that do not share a letter are significantly different.

Tukey Pairwise Comparisons: Status

Grouping Information Using the Tukey Method and 95% Confidence

Status	N	Mean	Grouping
Run	6	55.8333	A
Idle	2	41.5000	A

Means that do not share a letter are significantly different.

Tukey Pairwise Comparisons: Active Cooling*Status

Grouping Information Using the Tukey Method and 95% Confidence

Active Cooling*Status	N	Mean	Grouping
N Run	3	69.0000	A
N Idle	1	43.0000	A
Y Run	3	42.6667	A
Y Idle	1	40.0000	A

Means that do not share a letter are significantly different.

WORKSHEET 1

Comparisons for PCB - Heat Sink

Tukey Pairwise Comparisons: Active Cooling

Grouping Information Using the Tukey Method and 95% Confidence

Active Cooling	N	Mean	Grouping
N	4	32.5	A
Y	4	25.5	B

Means that do not share a letter are significantly different.

Tukey Pairwise Comparisons: Status

Grouping Information Using the Tukey Method and 95% Confidence

Status	N	Mean	Grouping
Run	6	31	A
Idle	2	27	A

Means that do not share a letter are significantly different.

Tukey Pairwise Comparisons: Active Cooling*Status

Grouping Information Using the Tukey Method and 95% Confidence

Active Cooling*Status	N	Mean	Grouping
N Run	3	35	A
N Idle	1	30	A
Y Run	3	27	A
Y Idle	1	24	A

Means that do not share a letter are significantly different.

WORKSHEET 1

Comparisons for PCB - Open Space

Tukey Pairwise Comparisons: Active Cooling

Grouping Information Using the Tukey Method and 95% Confidence

Active Cooling	N	Mean	Grouping
N	4	35.3333	A
Y	4	27.6667	B

Means that do not share a letter are significantly different.

Tukey Pairwise Comparisons: Status

Grouping Information Using the Tukey Method and 95% Confidence

Status	N	Mean	Grouping
Run	6	38.5	A
Idle	2	24.5	B

Means that do not share a letter are significantly different.

Tukey Pairwise Comparisons: Active Cooling*Status

Grouping Information Using the Tukey Method and 95% Confidence

Active Cooling*Status	N	Mean	Grouping
N Run	3	46.6667	A
Y Run	3	30.3333	B
Y Idle	1	25.0000	B
N Idle	1	24.0000	B

Means that do not share a letter are significantly different.

REFERENCES

[1] A. L. Mora Carpio and J. I. Mora, "Ventilator Management," in *StatPearls*, Treasure Island, Florida: StatPearls Publishing, 2020.

[2] P. L. Silva and P. R. M. Rocco, "The basics of respiratory mechanics: ventilator-derived parameters," *Annals of Translational Medicine,* vol. 6, no. 19, p. 376, 2018.

[3] H. Glass, "High-Acuity Ventilator Cost Guide," Medtronic, 2019. [Online]. Available: https://hcpresources.medtronic.com/blog/high-acuity-ventilator-cost-guide. [Accessed 11 May 2021].

[4] A. De Crescentis, "HCP Resources," Medtronic, 2018. [Online]. Available: https://hcpresources.medtronic.com/blog/how-much-do-vents-cost-in-the-sub-acute-setting. [Accessed 11 May 2021].

[5] G. Neyman and C. B. Irvin, "A single ventilator for multiple simulated patients to meet disaster surge," *Academic Emergency Medicine,* vol. 13, no. 11, pp. 1246-1249, 2006.

[6] K. Menes, J. Tintinalli and L. Plaster, "How One Las Vegas ED Saved Hundreds of Lives After the Worst Mass Shooting in U.S. History," Emergency Physicians Monthly, 3 November 2017. [Online]. Available: https://epmonthly.com/article/not-heroes-wear-capes-one-las-vegas-ed-saved-hundreds-lives-worst-mass-shooting-u-s-history/. [Accessed 11 May 2021].

[7] M. L. Ranney, V. Griffeth and A. K. Jha, "Critical Supply Shortages - The Need for Ventilators and Personal Protective Equipment during the Covid-19 Pandemic," *New England Journal of Medicine,* vol. 382, no. 18, p. e41, 2020.

[8] M. I. Meltzer, A. Patel, A. Ajao, S. V. Nystrom and L. M. Koonin, "Estimates of the Demand for Mechanical Ventilation in the United States During an Influenza Pandemic," *Clinical Infectious Diseases,* vol. 60, no. Suppl 1, pp. S52-S57, 2015.

[9] D. Patrone and D. Resnik, "Pandemic Ventilator Rationing and Appeals Processes," *Health Care Analysis,* vol. 19, no. 2, pp. 165-179, 2011.

[10] D. Campbell, "NHS hospitals facing serious shortages of vital equipment," The Guardian, 25 January 2018. [Online]. Available: https://www.theguardian.com/society/2018/jan/25/nhs-hospitals-serious-shortages-vital-equipment. [Accessed 11 May 2021].

[11] V. Krishnamoorthy, M. S. Vavilala and C. N. Mock, "The need for ventilators in the developing world: An opportunity to improve care and save lives," *Journal of Global Health,* vol. 4, no. 1, p. 010303, 2014.

[12] P. Zhou, X.-L. Yang, X.-G. Wang, B. Hu, L. Zhang, W. Zhang, H.-R. Si, Y. Zhu, C.-L. Huang, H.-D. Chen, J. Chen, y. Luo, H. Guo, R.-D. Jiang, M.-Q. Liu, Y. Chen, X.-R. Shen, X. Wang, X.-S. Zheng, K. Zhao, Q.-J. Chen, F. Deng, L.-L. Liu, B. Yan, F.-X. Zhan, Y.-Y. Wang, G.-F. Xiao and

Z.-L. Shi, "A pneumonia outbreak associated with a new coronavirus of probable bat origin," *Nature,* vol. 579, pp. 270-273, 2020.

[13] M. Cascella, M. Rajnik, A. Aleem, S. C. Dulebohn and R. Di Napoli, "Features, Evaluation, and Treatment of Coronavirus (COVID-19)," in *StatPearls,* Treasure Island, Florida: StatPearls Publishing, 2021.

[14] Center for Disease Control and Prevention, "Clinical Care Guidance," Centers for Disease Control and Prevention, 16 February 2021. [Online]. Available: https://www.cdc.gov/coronavirus/2019-ncov/hcp/clinical-guidance-management-patients.html. [Accessed 11 May 2021].

[15] K. Iyengar, S. Bahl, R. Vaishya and A. Vaish, "Challenges and solutions in meeting up the urgent requirement of ventilators for COVID-19 patients," *Diabetes & Metabolic Syndrome,* vol. 14, no. 4, pp. 499-501, 2020.

[16] N. Akbulaev, I. Mammadov and V. Aliyev, "Economic Impact of COVID-19," *SYLWAN,* vol. 164, no. 5, p. ISI Indexed, 2020.

[17] E. Reynolds and E. McSweeney, "'Desperate' shortage of ventilators for coronavirus patients put manufacturers on wartime footing," CNN Business, 19 March 2020. [Online]. Available: https://www.cnn.com/2020/03/19/business/coronavirus-ventilators-manufacture-intl/index.html. [Accessed 11 May 2021].

[18] B. Perrigo, "How Countries Around the World Are Helping India Fight COVID-19 - and How You Can Too," TIME, 26 April 2021. [Online]. Available: https://time.com/5958725/india-covid-19-world-aid/. [Accessed 11 May 2021].

[19] J. Banerjee, "Covid-19 second wave: Why are hospitals falling short of ventilators, again?," Forbes India, 9 April 2021. [Online]. Available: https://www.forbesindia.com/article/take-one-big-story-of-the-day/covid19-second-wave-why-are-hospitals-falling-short-of-ventilators-again/67381/1. [Accessed 11 May 2021].

[20] World Health Organization, "WHO Coronavirus (COVID-19) Dashboard," 10 May 2021. [Online]. Available: https://covid19.who.int/.

[21] Centers for Disease Control and Prevention, "About the Variants," Centers for Disease Control and Prevention, 2 April 2021. [Online]. Available: https://www.cdc.gov/coronavirus/2019-ncov/transmission/variant.html. [Accessed 11 May 2021].

[22] E. Bendavid, T. Ottersen, L. Peilong, R. Nugent, N. Padian, J.-A. Rottingen and M. Schaferhoff, "Development Assistance for Health," in *Disease Control Priorities: Improving Health and Reducing Poverty*, 3rd ed., Washington, District of Columbia: The International Bank for Reconstruction and Development/The World Bank, 2017, p. Chapter 16.

[23] J. T. Bucher, R. Vashisht, M. Ladd and J. S. Cooper, "Bag Mask Ventilation," in *StatPearls,* Treasure Island, Florida: StatPearls Publishing, 2020.

[24] J. D. Davies, B. K. Costa and A. J. Asciutto, "Approaches to Manual Ventilation," *Respiratory Care,* vol. 59, no. 6, pp. 810-814, 2014.

[25] A. Khoury, A. De Luca, F. S. Sall, L. Pazart and G. Capellier, "Performance of manual ventilation: how to define its efficiency in bench studies? A review of the literature," *Anaesthesia,* vol. 70, pp. 985-992, 2015.

[26] P. L. Wang and S. C. Brooks, "Mechanical versus manual chest compressions for cardiac arrest," *The Chochrane Database of Systematic Reviews,* vol. 8, no. 8, p. CD007260, 2018.

[27] J. G. Betts, K. A. Young, J. A. Wise, E. Johnson, B. Poe, D. H. Kruse, O. Korol, J. E. Johnson, M. Womble and P. DeSaix, "The Respiratory System," in *Anatomy and Physiology*, Houston, Texas: OpenStax, 2013.

[28] R. Chaudhry and B. Bordoni, "Anatomy, Thorax, Lungs," in *StatPearls*, Treasure Island, Florida: StatPearls Publishing, 2021.

[29] S. Fowler, R. Roush and J. Wise, "Circulatory and Respiratory Systems," in *Concepts of Biology*, Houston, Texas: OpenStax, 2013.

[30] J. G. Betts, K. A. Young, J. A. Wise, E. Johnson, B. Poe, D. H. Kruse, O. Korol, J. E. Johnson, M. Womble and P. DeSaix, "The Lungs," in *Anatomy and Physiology*, Houston, Texas: OpenStax, 2013.

[31] K. Neupane and R. T. Jamil, "Physiology, Transpulmonary Pressure," in *StatPearls*, Treasure Island, Florida: StatPearls Publishing, 2020.

[32] K. A. Powers and A. S. Dhamoon, "Physiology, Pulmonary Ventilation and Perfusion," in *StatPearls*, Treasure Island, StatPearls Publishing, 2020.

[33] P. D. Wagner, R. B. Laravuso, R. R. Uhi and J. B. West, "Continuous Distributions of Ventilation-Perfusion Ratios in Normal Subjects Breathing Air adn 100% O2," *Journal of Clinical Investigation,* vol. 54, no. 1, pp. 54-68, 1974.

[34] K. Brandis, The Physiology Viva: Questions and Answers, Willow Vale, Queensland: Alderbury House, 1997.

[35] J. H. Bates, "Systems Physiology of the Airways in Health and Obstructive Pulmonary Disease," *Wiley Interdisciplinary Reviews: System Biology and Medicine,* vol. 8, no. 5, pp. 423-437, 2017.

[36] J. J. Hurley and J. L. Hensley, "Physiology, Airway Resistance," in *StatPearls*, Treasure Island, Florida: StatPearls Publishing, 2020.

[37] M. Quinn, K. St Lucia and A. Rizzo, "Anatomy, Anatomic Dead Space," in *StatPearls*, Treasure Island, Florida: StatPearls Publishing, 2021.

[38] S. Intagliata, A. Rizzo and W. G. Gossman, "Physiology, Lung Dead Space," in *StatPearls*, Treasure Island, Florida: StatPearls Publishing, 2020.

[39] H. T. Robertson, "Dead space: the physiology of wasted ventilation," *European Respiratory Journal,* vol. 45, pp. 1704-1716, 2015.

[40] J. P. Desai and F. Moustarah, "Pulmonary Compliance," in *StatPearls*, Treasure Island, Florida: StatPearls Publishing, 2020.

[41] Z. Edwards and P. Annamaraju, "Physiology, Lung Compliance," in *StatPearls*, Treasure Island, Florida: StatPearls Publishing, 2020.

[42] B. D. Seadler, F. Toro and S. Sharma, "Physiology, Alveolar Tension," in *StatPearls*, Treasure Island, Florida: StatPearls Publishing, 2020.

[43] H. D. Prange, "Laplace's law and the alveolus: a misconception of anatomy adn a misapplication of physics," *Advances in Physiology Education,* vol. 27, no. 1-4, pp. 34-40, 2003.

[44] G. F. Nieman, H. Al-Khalisy, M. Kollisch-Singule, J. Satalin, S. Blair, G. Trikha, P. Andrews, M. Madden, L. A. Gatto and N. M. Habashi, "A Physiologically Informed Strategy to Effectively Open, Stabilize, and Protect the Acutely Injured Lung," *Frontiers in Physiology,* vol. 11, p. 227, 2020.

[45] G. Lista, F. Castoldi, S. Bianchi and F. Cavigioli, "Surfactant and mechanical ventilation," *Acta bio-medica: Atenei Parmensis,* vol. 83, no. Suppl 1, pp. 21-23, 2012.

[46] M. A. Matthay and R. L. Zemans, "The Acute Respiratory Distress Syndrome: Pathogenesis and Treatment," *Annual Review of Pathology: Mechanisms of Disease,* vol. 6, pp. 147-163, 2011.

[47] R. K. Albert, "The Role of Ventilation-induced Surfactant Dysfunction and Atelectasis in Causing Acute Respiratory Distress Syndrome," *American Journal of Respiratory and Critical Care Medicine,* vol. 185, no. 7, pp. 702-708, 2011.

[48] G. Grasselli, T. Tonetti, A. Protti, T. Langer, M. Girardis, G. Bellani, J. Laffey, G. Carrafiello, L. Carsana, C. Rizzuto, A. Zanella, V. Scaravilli, G. Pizzilli, D. L. Grieco, L. Di Meglio, G. de Pascale, E. Lanza, F. Monteduro, M. Zompatori, C. Filippini, F. Locatelli, M. Cecconi, R. Fumagalli, S. Nava, J.-L. Vincent, M. Antonelli, A. S. Slutsky, A. Pesenti, V. M. Ranieri and on behalf of the collaborators, "Pathophysiology of COVID-19-associated acute respiratory distress syndrome: a multicentre prospective observational study," *Lancet Respiratory Medicine,* vol. 8, pp. 1201-1208, 2020.

[49] S. Ranjeva, R. Pinciroli, E. Hodell, A. Mueller, C. C. Hardin, B. T. Thompson and L. Berra, "Identifying clinical and biochemical phenotypes in acute respiratory distress syndrome secondary to coronavirus disease-2019," *EClinicalMedicine,* vol. 34, p. 100829, 2021.

[50] K. Chandrasekaran and A. M. Shaji, "The role of a negative pressure ventilator coupled with oxygen helmet against COVID-19: a review," *Research on Biomedical Engineering,* 2021.

[51] V. Antonaglia, S. Pascotto and F. Piller, "Advanced Modalitities in Negative-Pressure Ventilation," in *Respiratory System and Artificial Ventilation*, Milan, Springer-Verlag Mailand, 2008, pp. 221-235.

[52] I. Potchileev, M. Doroshenko and A. N. Mohammed, "Positive Pressure Ventilation," in *StatPearls*, Treasure Island, Florida: StatPearls Publishing, 2020.

[53] J. V. Divatia, P. U. Khan and S. N. Myatra, "Tracheal intubation in the ICU: Life saving or life threatening?," *Indian Journal of Anaesthesia*, vol. 55, no. 5, pp. 470-475, 2011.

[54] J. X. Lian, "Understanding ventilator waveforms-and how to use them in patient care," *Nursing Critical Care*, vol. 4, no. 1, pp. 43-55, January 2009.

[55] A. L. Mora Carpio and J. I. Mora, "Positive End-Expiratory Pressure," in *StatPearls*, Treasure Island, Florida: StatPearls Publishing, 2020.

[56] M. Mittermaier, P. Pickerodt, F. Kurth, L. Bosquillon de Jarcy, A. Uhrig, C. Garcia, F. Machleidt, P. Pergantis, S. Weber, Y. Li, A. Breitbart, F. Bremer, P. Knape, M. Dewey, F. Doellinger, S. Weber-Carstens, A. S. Slutsky, W. M. Kuebler, N. Suttorp and H. Muller-Redetzky, "Evaluation of PEEP and prone positioning in early COVID-19 ARDS," *EClinicalMedicine*, vol. 28, p. 100579, 2020.

[57] C. Hoffmann, "Design and Control of a Novel Portable Mechanical Ventilator," Technical University of Hamburg-Harburg, Hamburg, 2011.

[58] S. Haribhai and S. K. Mahboobi, "Ventilator Complications," in *StatPearls*, Treasure Island, Florida: StatPearls Publishing, p. 2021.

[59] Ambu Inc., "Ambu(R) PEEP Disposable Valves," Ambu Inc., 2021. [Online]. Available: https://www.ambuusa.com/emergency-care-and-training/resuscitators/product/peep-valves. [Accessed 25 May 2021].